Exploring the sensitivity of atmospheric nitrate concentrations to nitric acid uptake rate using the Met Office's Unified Model

Anthony C. Jones[1], Adrian Hill[1], Samuel Remy[2], N. Luke Abraham[3,4], Mohit Dalvi[1], Catherine Hardacre[1], Alan J. Hewitt[1], Ben Johnson[1], Jane P. Mulcahy[1], and Steven T. Turnock[1,5]

[1] Met Office, Fitzroy Road, Exeter, EX1 3PB, UK
[2] HYGEOS, Lille, France
[3] National Centre for Atmospheric Science, U.K.
[4] Department of Chemistry, University of Cambridge, Lensfield Road, Cambridge, CB2 1EW, U.K.
[5] University of Leeds, Met Office Strategic Research Group, School of Earth and Environment, University of Leeds, Leeds, UK

Correspondence to: Anthony C. Jones (anthony.jones@metoffice.gov.uk)

Abstract.

Ammonium nitrate is a major aerosol constituent over many land regions and contributes to air pollution episodes, ecosystem destruction, regional haze, and aerosol-induced climate forcing. Many climate models that represent ammonium nitrate assume that the ammonium-sulphate-nitrate chemistry reaches thermodynamic equilibrium instantaneously without considering kinetic limitations on condensation rates. The Met Office's Unified Model (UM) is employed to investigate the sensitivity of ammonium nitrate concentrations to the nitric acid uptake coefficient (γ) in a newly developed nitrate scheme in which first order condensation theory is utilised to limit the rate at which thermodynamic equilibrium is attained. Two values of γ representing fast ($\gamma = 0.193$) and slow ($\gamma = 0.001$) uptake rates are tested in 20-year global UM integrations. The global burden of nitrate associated with ammonium in the 'fast' simulation (0.11 Tg[N]) is twice as great as in the 'slow' simulation (0.05 Tg[N]), while the top-of-the-atmosphere radiative impact of representing nitrate is -0.19 Wm^{-2} in the 'fast' simulation and -0.07 Wm^{-2} in the 'slow' simulation. In general, the 'fast' simulation exhibits better spatial correlation with observed nitrate concentrations while the 'slow' simulation better resolves the magnitude of concentrations. Local near-surface nitrate concentrations are found to be highly correlated with seasonal ammonia emissions suggesting that ammonia is the predominant limiting factor controlling nitrate prevalence. This study highlights the high sensitivity of ammonium nitrate concentrations to nitric acid uptake rates and provides a novel mechanism for reducing nitrate concentration biases in climate model simulations. The new UM nitrate scheme represents a step-change in aerosol modelling capability in the UK across weather and climate timescales.

1 Introduction

Air pollution poses a significant hazard to human-health and to the environment world-wide. In 2016, 90 % of the global population were exposed to pollutant concentrations in excess of World Health Organisation (WHO) defined safe levels, resulting in ~7 million premature deaths (WHO, 2020). Specific human-health conditions arising from air pollution exposure include lung cancer and cardiopulmonary disease, and deleterious impacts also extend to ecosystems (e.g. eutrophication, loss of biodiversity, acid deposition), building and infrastructure erosion, and impaired atmospheric visibility and regional haze (Kucera and Fitz, 1995; Monks *et al.*, 2009; Lovett *et al.*, 2009; Xu *et al.*, 2019). Solid or liquid particulate matter (PM) is a significant component of air pollution and particles with diameters less than 2.5 μm (i.e. $PM_{2.5}$) are particularly harmful to human health. Lelieveld *et al.* (2015) estimate $PM_{2.5}$ related global mortality to be 3.3 million deaths yr^{-1} in 2010, far greater than the second deadliest air pollutant, ozone (O_3, 142 thousand deaths yr^{-1}). Sources of air pollution differ with region; in North Africa and the Middle East, the predominant source is naturally emitted dust; in Europe, agricultural activity; and in South East Asia, residential energy production (Lelieveld *et al.*, 2015).

Secondary inorganic ammonium (NH_4), sulphate (SO_4), and nitrate (NO_3) aerosol form a major part of $PM_{2.5}$ composition in the Northern Hemisphere (Jiminez *et al*., 2009). Ammonium is predominantly emitted as ammonia (NH_3) gas by agricultural sources such as mineral fertilizer application and volatilization of livestock manure; biomass burning and from oceans (Bauer *et al*., 2016). NH_3 emissions from agriculture have dramatically increased since the discovery of the Haber-Bosch process for extracting reactive nitrogen from its stable atmospheric form (N_2) in the early 20th Century. The corresponding NH_3-based fertilizer revolution led to significantly enhanced global food production and a population explosion from 2 billion to 7 billion people (Smith *et al*., 2020). However, reactive nitrogen deposition from fertiliser usage is now 20-fold higher than it was before the industrial revolution, leading to environmental degradation (Xu *et al*., 2019). NO_3 is formed from atmospheric nitric acid (HNO_3), itself an oxidation product of nitrogen oxides (NO_x = NO + NO_2). NO_x is primarily emitted from anthropogenic fossil fuel burning (21-28 Tg N yr^{-1}) but has natural sources including soil emissions, biomass burning and lightning (12-35 Tg N yr^{-1}) (Seinfeld and Pandis, 1998; Vinken *et al.*, 2014). NO_x exacerbates air pollution via two pathways – by NO_3 aerosol production and by net O_3 production in the presence of sunlight and volatile organic compounds (VOCs) (Crutzen, 1970). SO_4 is the oxidation product of sulphur dioxide (SO_2), which is primarily emitted by anthropogenic processes such as fossil fuel combustion, petroleum refining, and metal smelting (Zhong *et al*., 2020). Natural SO_2 sources include volcanic degassing and the oxidation of reduced natural sulphurous compounds such as dimethyl sulphide (DMS) (Carn *et al*., 2017). Global anthropogenic SO_2 emissions have steadily declined from a peak of ~70 Tg S yr^{-1} in the 1980s to ~52 Tg S yr^{-1} in 2014 owing to clean air regulation instigated to mitigate adverse SO_2 impacts such as acid rain and also for human health benefits (Mcduffie *et al.*, 2020; Zhong *et al*., 2020). Global NO_x emissions peaked in 2010 at ~40 Tg N yr^{-1}, with emissions growth from 1990-2010 driven by rapid industrialisation in Asia and intensified international shipping, but have decreased by 7 % over the 2010s owing primarily to traffic emission control measures in China (Mcduffie *et al*., 2020).

In the troposphere, NO_x is involved in a complex diurnal photochemical cycle involving VOCs and O_3. The dominant NO_x removal mechanism during daytime is via oxidation by hydroxyl (OH) radicals to form HNO_3 (Seinfeld and Pandis, 1998). At night-time, NO_2 is unable to photolyze and the dominant NO_x removal mechanism is via reaction with O_3 to produce the NO_3 radical; which further reacts with NO_2 to form dinitrogen pentoxide (N_2O_5); which heterogeneously reacts with water (H_2O) to produce HNO_3 (Atkinson, 2000). HNO_3 is highly soluble and rapidly dissolves in water droplets or is neutralised by NH_3 to form aerosol. SO_2 is oxidised in the aqueous phase by dissolved oxidants such as O_3 and hydrogen peroxide (H_2O_2), and in the gas phase by OH, to form non-volatile H_2SO_4 (Seinfeld and Pandis, 1998). H_2SO_4 and HNO_3 react with NH_3 to produce ammonium sulphate ($(NH_4)_2{\cdot}SO_4$) and semi-volatile ammonium nitrate ($NH_4{\cdot}NO_3$) aerosol respectively, with H_2SO_4 neutralisation taking precedence owing to the lower vapor pressure of H_2SO_4 over HNO_3 (Hauglustaine *et al.*, 2014). In a slower process, HNO_3 also condenses irreversibly onto existing dust and sea-salt aerosols, forming calcium nitrate ($Ca{\cdot}(NO_3)_2$) and sodium nitrate ($Na{\cdot}NO_3$) salts respectively (Li and Shao, 2009). Owing to the prevalence of anthropogenic NO_x and NH_3 sources, particulate NO_3 is a major component of urban air pollution. For example, in Europe NO_3 constitutes 17 % of urban $PM_{2.5}$ aerosol by mass (Putaud *et al*., 2004), while $NH_4{\cdot}NO_3$ can comprise 75 % of $PM_{2.5}$ in air pollution events in Salt Lake City (Womack *et al.*, 2019).

Nitrate aerosol has an enigmatic history within the climate modelling community owing to the complexity of modelling HNO_3 neutralisation by NH_3 and the semi-volatility of $NH_4{\cdot}NO_3$ aerosol. In the inorganic aerosol system, gaseous and particulate equilibria are reached at different rates due to evolving temperature and acidity constraints, and the variability in gaseous uptake with particle size (Myhre *et al.*, 2006; Benduhn *et al*., 2016). Although complex dynamical and 'hybrid dynamical' schemes that fully or partially resolve the chemistry of inorganic aerosol exist (e.g. Jacobson, 1997; Feng and Penner, 2007; Zaveri *et al.*, 2007; Benduhn *et al*., 2016; Xu and Penner, 2012), they remain computationally expensive – owing to the numerical stiffness of the inorganic system – when compared to schemes that assume thermodynamic equilibrium is reached instantaneously (Nenes *et al*., 1998). Most of the current crop of nitrate-resolving global climate models (GCMs) and some regional climate models (RCMs) assume the instantaneous thermodynamic equilibrium approximation (Liao *et al*., 2003; Myhre *et al*., 2006; Bauer *et al*., 2007; Bellouin *et al.*, 2011; Hauglustaine *et al*., 2014; Paulot *et al*., 2016; Bian *et al*., 2017; Remy *et al.*, 2019). Dynamical models have the advantage of capturing natural phenomena where the inorganic aqueous system is outside of (or slow to reach) equilibrium, for instance in low gas concentrations, low temperatures, high Relative Humidities (RH), and for condensation onto coarse particles (Wexler and Seinfeld, 1990; Benduhn *et al*., 2016). Thermodynamic equilibrium models typically overestimate the fraction of NO_3 in the coarse mode, for example, in one study NO_3 associated with fine mode $NH_4{\cdot}NO_3$ was underestimated by 25 % compared to a hybrid-dynamical model (Feng and Penner, 2007). However, the additional computational expense of using dynamical approaches has motivated the climate modelling community to seek pragmatic solutions to represent NH_4 and NO_3 aerosol in GCMs and RCMs.

GCM simulations suggest that the present-day direct radiative forcing from NO_3 (global mean ≈ -0.1 Wm^{-2}) amounts to a quarter of the SO_4 forcing on a global-mean basis (Myhre *et al*., 2006; Bauer *et al*., 2007; Bellouin *et al*., 2011; Hauglustaine *et al*., 2014). NO_3 aerosol burdens are widely projected to increase over the 21st century as a result of stricter SO_2 emissions regulations and continued elevated NH_3 emissions, which would reduce the SO_4 available for neutralisation and concomitantly liberate NH_4 for $NH_4{\cdot}NO_3$ formation (Bauer *et al*., 2007; Bellouin *et al*., 2011). Consequently, NO_3 may become the dominant aerosol species in terms of radiative and urban air pollution impact by the end of the century, depending on future emissions of SO_2, NH_3 and NO_x (Hauglustaine *et al*., 2014). Such NO_3 concentration enhancements may be effectively mitigated on a regional basis by judicious regulation targeting anthropogenic NH_3 and/or NO_x emissions (Bauer *et al*., 2016). However, climate models disagree as to whether near-surface NO_3 concentrations will increase or decrease in future climate, and on the correct partitioning between NO_3 in the fine mode (associated with NH_4) and coarse mode (associated with dust and sea-salt) (Bian *et al*., 2017). Many of the uncertainties in NH_4 and NO_3 projections emanate from different treatments of the HNO_3 and NH_3 gases in models, with Bian *et al.* (2017) highlighting wet deposition as a particularly sensitive process. Additionally, the vertical distributions of HNO_3 and NH_3 are poorly constrained by observations which adds to uncertainty in NH_4 and NO_3 projections (Paulot *et al.*, 2016).

The emerging conclusion from observations and from the burgeoning literature on nitrate modelling is that ammonium nitrate poses an increasingly significant health hazard through urban air pollution (e.g. DEFRA, 2012) and via deposition to nitrogen-saturated ecosystems (Li *et al.*, 2016); and potentially could become a major climate forcing agent as SO_4 concentrations wane (Hauglustaine *et al.*, 2014). The impetus for explicitly representing NH_4 and NO_3 in GCMs is clear, even by using simple thermodynamic equilibrium approaches which bypass temporal nuances in the gas-particulate partitioning. The Met Office Unified Model (UM) has previously incorporated a thermodynamic-equilibrium ammonium nitrate scheme in the CMIP5-generation climate model Hadley Centre Global Environment Model version 2 (HadGEM2-ES) (Bellouin *et al.*, 2011). This nitrate scheme – developed within the single-moment Coupled Large-scale Aerosol Simulator for Studies in Climate (CLASSIC) aerosol framework (Bellouin *et al.*, 2007) – continues to be utilised for online air quality forecasts across the UK in the operational Air Quality Unified Model (AQUM) (Savage *et al.*, 2013). However, the CMIP6-generation state-of-the-art United Kingdom Earth System Model version 1 (UKESM1) which incorporates the Global Atmosphere model vn7.1 (GA7.1) (Walters *et al.*, 2019) replaced the single-moment CLASSIC aerosol scheme with the double-moment Global Model of Aerosol Processes modal (GLOMAP-mode) scheme which currently omits ammonium nitrate (Mann *et al.*, 2010; Mulcahy *et al.*, 2020). Mulcahy *et al.* (2020) attributed a negative bias in aerosol optical depth and mass burden over northern hemisphere continents in UKESM1 to the missing NH_4 and NO_3. The hybrid-dynamical nitrate scheme developed by Benduhn *et al.* (2016) in the standalone GLOMAP-mode model is not currently implemented in the UM. This has provided the Met Office with fresh impetus to develop a simplified thermodynamic equilibrium nitrate scheme within the GLOMAP-mode framework for interim use in the UM and possible implementation in future generations of UKESM, in order to address the gaps in modelled NH_4

and NO_3 with their respective observations. The nitrate scheme may garner further utility if AQUM or its successor transitions to utilising the GLOMAP-mode aerosol scheme rather than CLASSIC (Hemmings and Savage, 2018).

In this paper we describe the development and testing of a simple thermodynamic equilibrium nitrate scheme in the UM and explore the sensitivity of the scheme to a key parameter that is poorly constrained by observations – the HNO_3 uptake coefficient on aerosol surfaces (γ). Specifically, most models assume that $NH_4{\cdot}NO_3$ concentrations reach thermodynamic equilibrium instantaneously without considering kinetic limitations on the condensation of HNO_3 or NH_3 onto existing aerosol particles, as is considered here. This is the first study to investigate the sensitivity of $NH_4{\cdot}NO_3$ concentrations to the HNO_3 uptake coefficient and provide an efficient method for reducing NO_3 concentration biases in GCMs. The UM nitrate scheme reported here comprises fine NH_4 and NO_3 aerosol in the Aitken, accumulation, and coarse soluble modes and coarse NO_3 representing NO_3 aerosol associated with dust and sea-salt in the accumulation and coarse soluble modes. The scheme was originally developed by Hauglustaine *et al*. (2014) for use in the LMDZ-INCA climate model, then adapted for ECMWF's version of GLOMAP-mode by Remy *et al.* (2019), following which it was kindly provided to the Met Office for adaptation to the UM. In Section 2.1, we describe the configuration of the UM used to test the new nitrate scheme. In Section 2.2, we describe the thermodynamic equilibrium nitrate model in detail. In Section 2.3 we describe the simulations performed in this study. In Section 3, we evaluate the model using surface and satellite observations and investigate the sensitivity of the model to perturbations to a key parameter – the HNO_3 uptake coefficient (γ) – in a manner analogous to Bauer *et al.* (2004). In Section 4, we discuss the utility of the nitrate scheme and provide a roadmap for future development and integration within UKESM.

2 Methods

2.1 The Met Office Unified Model (UM)

The nitrate scheme was originally developed using the UM with the science configurations Global Atmosphere vn7.1 (GA7.1) and Global Land vn7.0 (GL7.0) (Walters *et al*, 2019). Although the UM can be run at various resolutions, the resolution used here is the climate configuration N96L85, i.e. 1.875^o longitude by 1.25^o latitude with 85 vertical levels up to a model lid at 80 km, with 50 levels below 18 km altitude, and a model timestep of 20 mins (Walters *et al*, 2019). Further details of the UM configuration are provided in Section S1 in the Supplement.

In the model configuration used here, GA7.1 includes the United Kingdom Aerosol and Chemistry (UKCA) model which simulates atmospheric composition in the Earth System, with UKCA chemistry called once per model hour in N96L85, although emissions are evaluated every model timestep (Archibald *et al*., 2020). UKCA is coupled to the GLOMAP-mode aerosol scheme, permitting a holistic and prognostic treatment of aerosol and chemical processes over the entire atmosphere (Mann *et al*., 2010; Mulcahy *et al*., 2020). The coupled UKCA and GLOMAP-mode model is widely referred to as UKCA-mode. The Met Office's Hadley Centre Global Climate version 3.1 (HadGEM3-GC3.1) model – the physical basis of UKESM1

– uses a simplified UKCA chemistry configuration with important oxidants (O_3, OH, NO_3, HO_2) prescribed as monthly mean climatologies (Walters *et al*., 2019; Mulcahy *et al*., 2020). This is of insufficient complexity for ammonium nitrate aerosol, given the importance of missing gases (i.e. HNO_3, NH_3 and precursors) and chemical reactions. Instead the combined Stratospheric-Tropospheric version 1.0 (StratTrop 1.0) chemistry scheme, which is included in UKESM1 (Sellar *et al.*, 2019) and described in detail by Archibald *et al*. (2020), is utilised here. Although not mentioned in Archibald *et al*. (2020), gaseous ammonia (NH_3) is a passive tracer in StratTrop1.0, while gaseous nitric acid (HNO_3) is the product of various atmospheric chemical reactions (see Table S1 in the Supplement). Further details of the nitrogen chemistry in StratTrop1.0 is provided in Section 2.2. Gaseous dissolution in cloud droplets is modelled using the effective Henry's law framework, with UKCA uniformly assuming a fixed cloud water pH of 5.0. We address the assumption of a fixed pH in the Discussion (Section 4). Values required to calculate the effective Henry's law coefficients are specified as $K_H(298K) = 2.1\times10^5$, 1.23, and 1×10^6 for HNO_3, SO_2 and NH_3 respectively, and $-\Delta H/R = 8700$, 3020, and 0 K^{-1} for HNO_3, SO_2 and NH_3 respectively (Archibald *et al*., 2020). The values for NH_3 are comparable to AeroCom phase III values given in Table 5 in Bian *et al.* (2017).

Aerosol Mode	**Geometric mean diameter $\bar{D}$ (nm)**	**Geometric standard deviation σ_g**	**Species**
Nucleation soluble	1 – 10	1.59	SO_4, OM
Aitken soluble	10 – 100	1.59	SO_4, BC, OM, NH_4, NO_3
Accumulation soluble	100 – 1000	1.4	SO_4, BC, OM, SS, NH_4, NO_3, coarseNO_3
Coarse soluble	> 1000	2.0	SO_4, BC, OM, SS, NH_4, NO_3, coarseNO_3
Aitken insoluble	10 - 100	1.59	BC, OM

Table 1: Properties of the aerosol size distribution in the nitrate UKCA-mode setup including the size range of the modes, the geometric standard deviation, and the permitted aerosol species in each mode. Species include sulphate (SO_4), black carbon (BC), organic matter (OM), sea-salt (SS) and the newly added ammonium (NH_4), nitrate (NO_3) and coarse nitrate (coarseNO_3). Adapted from Table 1 in Mulcahy *et al*. (2020).

GLOMAP-mode is a prognostic double-moment aerosol scheme that carries aerosol mass and number concentrations in 4 soluble lognormal modes spanning sub-micron to super-micron sizes (nucleation, Aitken, accumulation, and coarse), as well an insoluble Aitken mode (see Table 1) (Mann *et al*., 2010; Mulcahy *et al*., 2020). The variable size distribution allows the median dry radius to evolve within prescribed size brackets, while the lognormal standard deviation or 'mode width' is held fixed. GA7.1's default GLOMAP-mode configuration includes the aerosols sulphate (SO_4), black carbon (BC), organic matter (OM), and sea-salt (SS), with species in each mode treated as an internal mixture. Mineral dust is represented in GA7.1 by the CLASSIC 6 bin scheme described by Woodward *et al*. (2001). Aerosol water content is simulated prognostically using the

Zdanovskii-Stokes-Robinson (ZSR) method, allowing for a more accurate representation of aerosol-cloud interactions and aerosol radiative impact than in CLASSIC. The direct aerosol radiative effect is modelled using UKCA-Radaer, which utilises pre-determined look-up tables of Mie extinction parameters based on aerosol size and composition (Bellouin *et al.*, 2013).

2.2 Nitrate model

In addition to the standard aerosols in GA7.1 - SO_4, BC, OM, and SS - ammonium (NH_4), nitrate (NO_3) and coarse nitrate (herein denoted coarseNO_3 for convenience) are added to a new UKCA-mode setup which comprises 28 aerosol tracers in total (Table 1). Note that 'NO_3' refers solely to NO_3 associated with NH_4, while 'coarseNO_3' refers to NO_3 associated with dust and sea-salt. NH_4 and NO_3 mass is emitted into the Aitken and accumulation soluble modes and may be transferred to the coarse soluble mode via aerosol processing, while coarseNO_3 is limited to the accumulation and coarse soluble modes. Nitrate chemistry is evaluated once per model timestep within the UKCA emissions-control routine. The nitrate model closely follows Hauglustaine *et al.* (2014) and Remy *et al.* (2019) with subtle yet important differences. An exhaustive step-by-step methodology is provided in the Supplement (Sections S2 and S3) and outlined below.

2.2.1 Ammonium nitrate production

Fine mode ammonium nitrate production is evaluated before the condensation of HNO_3 onto coarse aerosols (e.g. sea-salt and dust) because smaller particles generally reach thermodynamic equilibrium faster (Hauglustaine *et al.*, 2014; Benduhn *et al.*, 2016). Firstly, the sulphate neutralisation state (Γ_{SO_4}) is determined from the total moles of ammonia ($T_A = \{NH_3\} + \{NH_4^+\}$) and total moles of sulphate ($T_S = \{SO_4\}$) using Eq. 1 (Metzger *et al.*, 2002).

$$\Gamma_{SO_4} = \begin{cases} 2 & 2\,T_S < T_A & 2NH_3 + H_2SO_4 \rightarrow (NH_4)_2SO_4 \\ 1.5 & T_S < T_A < 2\,T_S & 3NH_3 + 2H_2SO_4 \rightarrow (NH_4)_3H(SO_4)_2 \\ 1 & T_A < T_S & NH_3 + H_2SO_4 \rightarrow (NH_4)HSO_4 \end{cases} \quad [1]$$

The moles of ammonia available for neutralisation of HNO_3 following the irreversible production of ammonium sulphate is then $T_A^* = T_A - \Gamma_{SO_4} T_S$. If all free ammonia is consumed by the neutralisation of SO_4 ($T_A^* = 0$) then no new nitrate is formed. However, if ammonia is available ($T_A^* > 0$) then the equilibrium constant (K_p) of the ammonia-nitrate system (Eq. 2) is determined using the parameterisation of Mozurkewich (1993) (see Section S2 in the Supplement). In this formulation, K_p is solely a function of temperature and Deliquescence Relative Humidity (DRH), with DRH following the parameterisation of Seinfeld and Pandis (1998).

$$HNO_3 + NH_3 \overset{K_p}{\leftrightarrow} NH_4NO_3 \quad [2]$$

The equilibrium concentration of ammonium nitrate is then calculated using the formulation from Seinfeld and Pandis (1998). Letting T_N denote the total molar concentration of nitrate ($T_N = \{HNO_3\} + \{NO_3^-\}$), if the available nitrate and ammonia suggest that the equilibrium of Reaction 2 is in the forwards direction, thereby promoting the condensation of HNO_3 and NH_3 to form NH_4NO_3 ($T_A^* T_N > K_p$), then the equilibrium concentration of NH_4NO_3 is solved using Eq. 3.. Else if free ammonia or nitrate concentrations are limited such that $T_A^* T_N \leq K_p$ or $T_A^* = 0$ then all existing ammonium nitrate aerosol evaporates and the corresponding mass is transferred to the gas phase HNO_3 and NH_3.

$$\{NH_4NO_3\}_{eq} = \frac{1}{2}\left[T_A^* + T_N - \sqrt{(T_A^* + T_N)^2 - 4\left(T_N T_A^* - K_p\right)}\right] \quad [3]$$

The ammonia-nitrate system may not reach equilibrium within a standard GCM timestep owing to transport limitations between the gas and aerosol phases (Wexler and Seinfeld, 1990). The time taken to reach equilibrium depends on ambient temperature and RH, and the aerosol size and uptake coefficient (γ), where the uptake coefficient is defined as the number of gas molecules condensing on a particle divided by the number impacting onto the particle surface. Ackerman *et al*. (1995) find that equilibration time (τ) may range from ~2 minutes for particles with diameters of 0.1 μm to ~1 hour for diameters of 0.5 μm, depending on the uptake rate. Remy *et al*. (2019) assumed a globally uniform equilibration time of $\tau = 2$ minutes in their nitrate model. Here the uptake rate k_{HNO3} is determined for each aerosol mode online (Aitken, accumulation, and coarse soluble) using the first order uptake theory of Schwartz (1986) and by applying the Fuchs and Sutugin (1970) correction factors for molecular effects and for limitations in interfacial mass transport (Eqs 4-7).

$$D_g = \frac{3}{8A_c\rho_a d_a^2}\left[\frac{m_a R_a T}{2\pi} \times \frac{m_a + m_{HNO3}}{m_{HNO3}}\right]^{\frac{1}{2}} \quad [4]$$

$$\lambda = \frac{3D_g}{\upsilon} = \frac{3D_g}{\sqrt{\frac{8R_a T}{\pi m_{HNO3}}}} \quad [5]$$

$$K_n = \frac{2\lambda}{D} \quad [6]$$

$$k_{HNO3} = \frac{2\pi D D_g}{1 + \frac{4K_n}{3\gamma} \times \left(1 - \frac{0.47\gamma}{1 + K_n}\right)} \quad [7]$$

Equations 4-7 determine the molecular diffusivity coefficient (D_g, $m^2 s^{-1}$), the mean free path (λ, m), the Knudsen number (K_n), and the modal condensation or uptake rate (k_{HNO3}, $m^3 s^{-1}$) respectively. Constants in the algorithm include the Avogadro constant $A_c = 6.022 \times 10^{23}$ mol^{-1}, the gas constant of dry air $R_a = 8.314$ J mol^{-1} K^{-1}, the molar mass of dry air $m_a = 0.029$ kg mol^{-1}, the molar mass of HNO_3 $m_{HNO3} = 0.063$ kg mol^{-1}, the molecular diameter of dry air molecules $d_a = 4.5 \times 10^{-10}$ m,

and the reactive uptake coefficient (γ) for HNO_3. Variables in Eqs 4-7 include the air temperature T (K) and air density ρ_a (kg m^{-3}). In Eq. 5, v is the mean molecular speed (m s^{-1}). The total equilibration time τ (s) may then be related to the inverse of product of the uptake rate for one particle k_{HNO3} and the aerosol number concentration N using Eq. 8. Note that ammonium nitrate production is limited to the Aitken and accumulation modes in this study, which is reflected in the formulation of τ.

$$\tau = \frac{1}{N_{ait} k_{HNO3,ait} + N_{acc} k_{HNO3,acc}} \quad [8]$$

Rather than assume instantaneous thermodynamic equilibrium in the ammonia-nitrate system, the model assumes an exponential decay of the gas phase towards equilibrium using the equilibration time τ (see Section S2.4 in the Supplement). This approach has also been used by Ackerman *et al.* (1995), Makar *et al.* (1998), and Remy *et al.* (2019). Figure S2 in the Supplement shows the results of applying the above algorithm for τ (with γ set to 0.193 following Feng and Penner (2007)) to monthly mean aerosol and meteorology output from example UM integrations. Over many land regions, τ is approximately 2 mins near the surface and increases to ~15 mins at a model level height of 3000 m. Therefore, assuming a constant value of $\tau = 2$ mins, as assumed by Remy *et al.* (2019), may significantly overestimate the rate which the ammonia-nitrate system approaches equilibrium, particularly at higher altitudes and over maritime regions. For example, in a 20-minute timestep the ammonia-nitrate system would move 99.995 % of the way from initial conditions towards equilibrium with $\tau = 2$ mins assuming exponential decay, but only 86 % of the way with $\tau = 10$ mins and 33 % of the way with $\tau = 50$ mins.

For standard atmospheric conditions ($D_g = 10^{-5}$ $m^2 s^{-1}$ and $v = 300$ ms^{-1}), k_{HNO3} scales approximately linearly with the reactive uptake coefficient γ, for γ from 0.001 to 0.2 and for particle diameters between $D = 0.1$ µm and $D = 5$ µm (Figure S3 in the Supplement). The uptake rate increases on a particle-by-particle basis with diameter, for example, ranging from 0.2 s^{-1} for $D = 0.1$ µm to 5 s^{-1} for $D = 0.5$ µm when $\gamma = 0.1$ and when k_{HNO3} is normalised by $N = 10^{12}$ m^{-3}. However, atmospheric Aitken mode number concentrations generally exceed accumulation mode concentrations, particularly over populous land regions and increasingly with altitude. Exceptions to this include near the surface over high-latitude maritime regions, Amazonia, and much of Australasia, where Accumulation number concentration exceed Aitken concentrations on an annual-mean basis in the UM. In example UM integrations, the ratio of accumulation to Aitken uptake ($N_{acc} k_{HNO3,acc} / N_{ait} k_{HNO3,ait}$) decreases on a global-mean basis from 8 at the surface to 1.4 at a model level height of 3000 m, but is effectively unity at the surface over key NH_3 and NO_x emitting regions such as the US, Europe and South Asia (Figure S4 in the Supplement).

Uptake rates (k_{HNO3}, Eq. 7) are determined for the Aitken and accumulation modes by using the modal geometric-mean dry diameters for D in Eqs 4-7, which are first corrected for hygroscopic growth using the RH-dependent parameterisation of Gerber *et al.* (1985). This simplified 'modal' approach differs from Hauglustaine *et al.* (2014) who divide aerosol size modes

into sub-bins. If the available nitrate and ammonia suggest that the equilibrium of Reaction 2 is in the forwards direction, thereby promoting the condensation of HNO_3 and NH_3 to form NH_4NO_3 ($T_A^* T_N > K_p$) then mass is transferred from the gaseous reactants NH_3 and HNO_3 to NH_4 and NO_3 in the Aitken and accumulation soluble modes using the above algorithm. Else if $T_A^* T_N \leq K_p$ then NH_4 and NO_3 dissociate and all NH_4 and NO_3 mass in the Aitken to coarse soluble modes is instantaneously transferred to the gas phase. Ammonium nitrate chemistry primarily involves condensation and evaporation (Makar *et al*., 1998; Benduhn *et al*., 2016), although Wang *et al.* (2020) have shown that NH_3 and HNO_3 can condense onto nanoparticles and thus contribute to nucleation events, which may be of importance in urban settings and at high altitudes. In this model, aerosol number concentrations are not altered explicitly by nitrate chemistry (assuming condensation and evaporation are more important than nucleation) but may change indirectly due to altered coagulation and mode-merging rates arising from the additional aerosol mass. This approach differs from Hauglustaine *et al*. (2014) and Remy *et al.* (2019) who assume that new particles are nucleated by the production of ammonium nitrate.

2.2.2 Coarse nitrate production

Following $NH_4{\cdot}NO_3$ production and the associated update to HNO_3 concentrations, the first order uptake parameterisation described by Eqs 4-7 is further employed to model the irreversible uptake of HNO_3 on sea-salt and dust to produce $NaNO_3$ (Eq. 9) and $Ca(NO_3)_2$ (Eq. 10) respectively (Liao *et al.*, 2003; Hauglustaine *et al*., 2014).

$$HNO_3 + NaCl \rightarrow NaNO_3 + HCl \quad [9]$$

$$2HNO_3 + CaCO_3 \rightarrow Ca(NO_3)_2 + H_2CO_3 \quad [10]$$

The methodology is mostly unchanged from Hauglustaine *et al*. (2014) and Remy *et al*. (2019), with only subtle adaptations needed to integrate the scheme within UKCA-mode. As in Hauglustaine *et al*. (2014), the HNO_3 uptake coefficients (γ) for dust and sea-salt are RH-dependent variables based on measurements from Fairlie *et al*. (2010) for dust and Sander *et al*. (2011) for sea-salt. Additionally, dust is assumed to uniformly constitute 5 % Ca^{2+} by mass as in Hauglustaine *et al*. (2014), which differs from the approach in Remy *et al*. (2019) who used a spatially hetereogeneous Ca^{2+} fraction more akin to observations. Dust alkalinity is titrated by uptake of HNO_3 until the dust pH is neutralised whereupon HNO_3 stops condensing [Fairlie *et al*., 2010; Hauglustaine *et al*., 2014], while no such limitation is necessary for sea-salt which generally constitutes a higher fraction of Na^+ ions per mass than dust constitutes Ca^{2+} [e.g. Xiao *et al.*, 2018].

As for the first order uptake parameterisation for ammonium nitrate (Section 2.2.1) and in Remy *et al.* (2019), rather than explicitly integrating the uptake rate over the aerosol size distribution, k_{HNO3} is calculated individually for sea-salt in the accumulation and coarse modes using the modal geometric-mean diameters for *D* in Eqs 4-7, and individually for each CLASSIC dust bin using fixed geometric mean diameters (see Section S3 in the Supplement). Sea-salt number concentrations

for the two modes are inversely determined from the sea-salt mass concentrations and the modal geometric-mean dry diameters, which implicitly assumes that sea-salt is externally mixed with other UKCA-mode aerosols. Dust particle number concentrations are determined from prognostic dust mass concentrations and fixed size distributions for each bin. Mapping between CLASSIC's 6 dust bins and UKCA-mode's 2 size modes follows the approach currently used to map dust emissions between CLASSIC and UKCA-mode, with Bin 2 and half of Bin 3 mapped to the accumulation mode and the other half of Bin 3 and Bins 4, 5 and 6 mapped to the coarse mode. The dust and sea-salt uptake rates (k) multiplied by the equivalent particle number concentrations (N) are then used to determine tendencies to mass concentrations of coarse NO_3 aerosol (coarseNO_3), sea-salt (SS), and HNO_3 gas (Eqs 11-13). The constants in Eqs 11-13 include the molar mass of $Ca(NO_3)_2$ $m_{Ca(NO3)2} = 0.164$ kg mol^{-1}, the molar mass of $NaNO_3$ $m_{NaNO3} = 0.084$ kg mol^{-1}, the molar mass of HNO_3 $m_{HNO3} = 0.063$ kg mol^{-1}, and the molar mass of NaCl $m_{NaCl} = 0.05844$ kg mol^{-1}.

$$\frac{\Delta[\text{coarseNO}_3]}{\Delta t} = \left(\left(Nk_{du,ACC} + Nk_{du,COA}\right) \times \frac{m_{Ca(NO3)2}}{m_{HNO3}} + \left(Nk_{SS,ACC} + Nk_{SS,COA}\right) \times \frac{m_{NaNO3}}{m_{HNO3}} \right) \times [\text{HNO}_3] \quad [11]$$

$$\frac{\Delta[\text{HNO}_3]}{\Delta t} = -\left(2 \times \left(Nk_{du,ACC} + Nk_{du,COA}\right) + \left(Nk_{SS,ACC} + Nk_{SS,COA}\right)\right) \times [\text{HNO}_3] \quad [12]$$

$$\frac{\Delta[\text{SS}]}{\Delta t} = -\left(Nk_{SS,ACC} + Nk_{SS,COA}\right) \times \frac{m_{NaCl}}{m_{HNO3}} \times [\text{HNO}_3] \quad [13]$$

2.2.3 Technical UM modifications

UKCA-Radaer calculates 3D aerosol extinction properties for each lognormal mode online as a function of aerosol composition and size, which are then utilised directly within the UM's radiative transfer code (Bellouin *et al*., 2013). Each aerosol species requires prescribed spectral refractive indices (RI) spanning the electromagnetic spectrum from ultra-violet (0.2 μm) to radiowave (1 cm) wavelengths. Ammonium nitrate RIs have previously been compiled for an older generation of the UM (HadGEM2-ES) (Bellouin *et al*., 2011). For $NH_4{\cdot}NO_3$, real and imaginary RIs for the wavelength spectrum 2-20 μm are taken from Jarzembski *et al*. (2003), while RIs for > 20 μm are assumed to be that at 20 μm. Real RIs for 0.59-1.61 μm are from CRC Handbook of Chemistry and Physics (Weast, 1971) and are then extended to cover the 0.1-2 μm spectrum. Imaginary RIs for the ultraviolet and visible spectra (< 0.7 μm) are arbitrarily set to a small number assuming little absorption (1×10^{-8}).

To optically represent the coarse NO_3 aggregate coarseNO_3, $NaNO_3$ spectral RIs have been compiled from the literature for this study. RI values are mostly from the tabulated data of Palik and Khanna (1998) and references therein for solid birefringent $NaNO_3$ crystals. From 0.23-0.42 μm, imaginary RIs are determined by applying the Beer-Lambert law to Cleaver *et al.* (1963) absorption coefficients and assuming a lattice thickness of 3 μm, as in Jacobson (1999). This approach is necessary to account for the second UV absorption peak missing in the data of Palik and Khanna (1998). Imaginary RIs for wavelength spectrum 0.42-5.88 μm appear not to have been measured and are pragmatically set to the observed values for $NH_4{\cdot}NO_3$, which are from

Gosse *et al.* (1997) for 0.7-2 µm and from Jarzembski *et al.* (2003) for 2-5.88 µm. As is the case for $NH_4{\cdot}NO_3$, imaginary RIs are set to an arbitrary small number (1×10^{-8}) from 0.42-0.7 µm to reflect the little or no absorption in that spectrum (Palik and Khanna, 1998). For the real RIs, in the 0.4-0.65 µm spectrum values are from Cotterell *et al.* (2017) for measurements at 0 % relative humidity. From 0.66-0.67 µm, the real RIs are provided by Ballard *et al.* (1972) and for 0.7 µm from Ivlev and Popova (1974). Above wavelengths of 1 mm - the scope of the Palik and Khanna (1998) database - the real and imaginary RIs are set to the value at 1 mm. The compiled spectral RIs for $NH_4{\cdot}NO_3$ and $NaNO_3$ are shown in Fig. S5 in the Supplement and tabulated in Tables S2 and S3 in the Supplement.

The default configuration of UKCA-mode and by extension UKCA-Radaer, as used in UKESM1 and HadGEM3-GC3.1, represents tropospheric SO_4 with $(NH_4)_2{\cdot}SO_4$ refractive indices and (optionally) stratospheric SO_4 with sulphuric acid (H_2SO_4) refractive indices. This is internally inconsistent given that the tropospheric SO_4 is missing the considerable mass associated with NH_4. The new UKCA-mode nitrate configuration presented here that includes SO_4, NO_3, and NH_4 as separate tracers firstly apportions NH_4 mass to NO_3 using a 1:1 molar ratio and the NH_4 remainder to SO_4 using a 2:1 molar ratio (represented by $NH_4{\cdot}NO_3$ and $(NH_4)_2{\cdot}SO_4$ refractive indices respectively), and then represents remaining SO_4 mass with H_2SO_4 refractive indices. Another internal inconsistency in the default UKCA-mode configuration is that NH_4 is not explicitly represented during hygroscopic growth (i.e. in the ZSR algorithm), owing to the lack of an NH_4 tracer. In the new nitrate scheme, NH_4, NO_3, and coarseNO_3 are explicitly added to the hygroscopic growth routine, with NH_4 counteracting hygroscopic aerosol growth and NO_3 and coarseNO_3 promoting it.

Simulation name	Description
CNTL	Control simulation - no nitrate aerosols
INSTANT	Nitrate aerosols – instantaneous equilibrium for NH_4NO_3 ($\tau = 0$ in Eq. 8)
FAST	Nitrate aerosols– fast uptake coefficient for NH_4NO_3 ($\gamma = 0.193$ in Eq. 7)
SLOW	Nitrate aerosols– slow uptake coefficient for NH_4NO_3 ($\gamma = 0.001$ in Eq. 7)

Table 2: A description of the UM simulations performed in this study

2.3 Simulation design

The scientific purpose of this study is to investigate whether representing the kinetic limitation of HNO_3 condensation onto pre-existing aerosols during the production of ammonium nitrate significantly alters the resulting atmospheric concentrations of ammonium nitrate and, indirectly, coarse nitrate aerosol. To this end, four sensitivity simulations are performed with the UM and the new nitrate scheme: 1. A control simulation with no nitrate aerosol and the default UKCA-mode setup 2 (i.e. standard GA7.1) (CNTL); 2. A simulation with $NH_4{\cdot}NO_3$ reaching equilibrium instantaneously (INSTANT); 3. A simulation

with the HNO_3 uptake rate set to $\gamma = 0.193$ in Eq. 7 following Feng and Penner (2007) (FAST); and 4. A simulation with the HNO_3 uptake rate set to $\gamma = 0.001$ in Eq. 7 following Bauer *et al.* (2007) (SLOW). These simulations are further listed in Table 2 and were selected to span the range of HNO_3 uptake rates on standard atmospheric particles from the literature (Bauer *et al.*, 2007). All simulations are run for 25 model years with only the last 20 years used for analysis.

In these simulations, GA7.1 is forced by fixed sea surface temperature and sea ice fields prescribed as monthly climatologies for the year 2000, created by averaging over 1995-2004 the time-series data generated for CMIP6 atmosphere-only simulations. Additionally, aerosol and gaseous emissions are primarily prescribed as monthly fields from the CMIP6 historical emissions inventory (DECK/ Historical CMIP6 version 6.2.0), averaged over the 1995-2004 time-period. Table S4 in the Supplement gives global and annual total emissions for each of the UKCA chemical species. The CMIP6 emissions inventory was derived from the Community Emissions Data System (CEDS) project which is documented by van Marle *et al.* (2017), Hoesly *et al.* (2018) and Feng *et al.* (2020); while its integration within the UM is detailed by Sellar *et al.* (2020). The simulation design (i.e. perpetual year 2000 conditions) follows standard simulation protocol for UKCA model development in the Met Office.

Global anthropogenic NH_3 emissions in the year 2000 from CEDS amount to 50 Tg yr^{-1}, in vast excess of equivalent emissions from the CMIP5-derived MACCitty inventory of 37.5 Tg yr^{-1} (Granier *et al.*, 2011). Hoesly *et al.* (2018) attribute this disparity to differing assumptions in agricultural NH_3 trends and to the lack of consideration for wastewater and human waste NH_3 emissions in MACCity. Such large discrepancies in NH_3 emissions inventories can impact direct model-measurement comparisons which make it important to consider the spatial and temporal trends in concentrations rather than just the overall magnitudes. For this work exploring the sensitivity of NH_4NO_3 to thermodynamic equilibrium assumptions, the direct comparison of model performance to observations is done with the goal of understanding the degree to which thermodynamic assumptions may push the model out of realistic behaviour rather than best re-creating the observations. Oceanic NH_3 emissions in these simulations – which account for 26 % of total NH_3 emissions – follow Bouwman *et al.* (1997) and biomass-burning emissions are described by van Marle *et al.* (2017). NH_3 exhibits a strong seasonal cycle with global emissions in June-August ~50 % greater than in December-February (Fig. S6b in the Supplement). The global NH_3 source of ~65 Tg yr^{-1} in these simulations is close to the model-mean value of 63 Tg yr^{-1} for GCMs participating in the AeroCom phase III nitrate experiment (Bian *et al.*, 2017). Nitrogen oxide (NO_x) emissions from anthropogenic, biomass-burning and aircraft sources are prescribed as monthly fields from the CEDS inventory (van Marle *et al.*, 2017; Hoesly *et al.*, 2018). NO_x emissions from soils are taken from Yienger and Levy (1995), corrected to a total source of 12 Tg[NO] yr^{-1} (Sellar *et al.*, 2020). The global and annual total NO_x emissions amount to 106 Tg[NO] yr^{-1}. Further details on gas and aerosol emissions in these simulations is provided in Section S4 in the Supplement.

3 Results

3.1 Global and annual mean metrics

Table 3 shows global tropospheric and annual mean budgets for HNO_3, NH_3, NO_3, and NH_4 from the FAST and SLOW simulations alongside equivalent metrics from the present day simulations of Xu and Penner (2012) (hereafter XP12), Hauglustaine *et al*. (2014) (hereafter HA14), and from the AeroCom model intercomparison project detailed by Bian *et al*. (2017) (hereafter BI17). The INSTANT simulation is near-indistinguishable from FAST using these metrics (Table S5 in the Supplement) - suggesting that $NH_4{\cdot}NO_3$ concentrations in FAST reach thermodynamic equilibrium near instantaneously - and INSTANT is thus omitted from further analysis. With respect to Table 3 and to the rest of the Results section, 'fine NO_3' refers to NO_3 associated with NH_4 while 'coarse NO_3' refers to NO_3 associated with dust and sea-salt (i.e. NO_3 in coarseNO_3).

The net HNO_3 production rates in FAST (44.1 Tg[N] yr^{-1}) and SLOW (44.2 Tg[N] yr^{-1}) are comparable to equivalent rates in HA14 (45.1 Tg[N] yr^{-1}) and XP12 (38 Tg[N] yr^{-1}). Additionally, the NH_3 emissions in FAST and SLOW (53.5 Tg[N] yr^{-1}) are comparable to HA14, XP12, and BI14 (50.5, 53.6, and 51.8 Tg[N] yr^{-1} respectively) suggesting that to the first order the ammonium and nitrate precursor gas emissions are commensurate on a global basis with prior studies. Total NO_3 (i.e. fine + coarse) production in the FAST (22.9 Tg[N] yr^{-1}) and SLOW (19.9 Tg[N] yr^{-1}) simulations is significantly greater than in HA14 (14.4 Tg[N] yr^{-1}) and XP12 (16 Tg[N] yr^{-1}) and at the upper range of the AeroCom models in BI17 (Mean = 13.7, Range = 1.5 to 28.2 Tg[N] yr^{-1}). This is also the case for NH_4 production rates where FAST (30.4 Tg[N] yr^{-1}) and SLOW (25.6 Tg[N] yr^{-1}) exceed equivalent values in HA14 (17.5 Tg[N] yr^{-1}) and BI17 (Mean = 23.7, Range = 17.8 to 29.5 Tg[N] yr^{-1}), and are comparable with XP12 (30.5 Tg[N] yr^{-1}). This suggests that NH_4 and NO_3 aerosol production in the UM is at the upper end of efficiency when compared to other existing climate models.

Significant differences between the FAST and SLOW simulations are highlighted by the global NO_3 metrics in Table 3. In particular, the fine NO_3 source is 6.3 Tg[N] yr^{-1} in FAST but only 2.7 Tg[N] yr^{-1} in SLOW, marking a 57 % decrease. Conversely, SLOW exhibits 5 % more coarse NO_3 production than in FAST, which is likely due to the surplus HNO_3 in SLOW owing to there being less fine NO_3 production. The difference is equally discernible in the burdens, with 47 % of the total NO_3 burden as coarse NO_3 in FAST compared to 67 % in SLOW. This can be compared to a 72 % coarse fraction in HA14 and 47 % in XP12, suggesting that the FAST and SLOW coarse fractions are between the instantaneous thermodynamic equilibrium model of HA14 and hybrid dynamical nitrate scheme of XP12. Note though that intuitively the coarse ratio in FAST would be expected to be close to HA14 (given that FAST is indistinguishable from the INSTANT simulation), whereas it is closer to XP12, which is probably due to differences in the precursor gas concentrations between FAST and HA14.

The total NO_3 burdens of 0.2 Tg[N] in FAST and 0.15 Tg[N] in SLOW are commensurate with 0.18 Tg[N] in HA14, 0.17 Tg[N] in XP12, and the AeroCom median of 0.14 Tg[N] in BI17. The NH_3 burden in FAST (0.04 Tg[N]) is at the lower end

of the AeroCom range in BI17 (0.04 to 0.7 Tg[N]) while the NH_4 burden in FAST (0.42 Tg[N]) is at the upper range of BI17 models (0.13 to 0.58 Tg[N]), suggesting that NH_3 is more rapidly neutralised to aerosol in the UM than in other GCMs. This corroborates the assertion that NH_4 and NO_3 aerosol production in the UM is at the upper end of efficiency when compared to other existing GCMs and suggests that NH_3 rather than HNO_3 is the limiting factor controlling NH_4NO_3 production in these simulations, given that the NH_3 burden in FAST is negligible. In summary, Table 3 illustrates the close parity with regards global and annual mean metrics between the UM simulations and previous nitrate simulations with various climate models from the literature and highlights the difference in fine NO_3 burdens between FAST and SLOW.

				FAST	**SLOW**	**XP12**	**HA14**	**BI17**
HNO_3	Source	Gas phase	Tg[N] yr^{-1}	35.2	35.7	24.4	44.6	[82, 92]
		Aerosol phase		18.6	18.2	17.9	3.9	[4.7, 28.5]
		Total		53.8	53.9	42.3	48.5	-
	Loss	Gas phase	Tg[N] yr^{-1}	9.7	9.7	4.3	3.4	[47, 66]
		Fine nitrate		6.4	2.7	8.8	3.2	[2, 9.5]
		Coarse nitrate		16.6	17.3	7.2	11.2	-
		Dry deposition		6	8	7.8	14.7	10.9 [8, 16.4]
		Wet deposition		14.9	15.8	14.5	17	25.1 [11, 37.2]
		Total		53.4	53.4	42.6	49.5	-
		Wet fraction	%	71.4	66.4	65	53.6	68.6 [57.8, 76.3]
	Burden		Tg[N]	0.48	0.48	0.3	0.3	0.56 [0.15, 1.27]
	Lifetime		days	3.2	3.2	4.8	2.3	[3.5, 5.7]
NO_3	Source	Fine nitrate	Tg[N] yr^{-1}	6.3	2.7	8.8	3.2	-
		Coarse nitrate		16.6	17.3	7.2	11.2	-
		Total		22.9	19.9	16	14.4	13.7 [1.5, 28.2]
	Loss	Dry deposition	Tg[N] yr^{-1}	8.9	8.3	4	1.7	4.7 [0.3, 10.8]
		Wet deposition		14.3	11.8	12	12.7	9.9 [1.2, 20.5]
		Total		23.2	20.1	16	14.4	13.7 [1.5, 28.3]
		Wet fraction	%	61.7	58.6	75	88.2	77 [56.3, 90.8]
	Burden	Fine nitrate	Tg[N]	0.11	0.05	0.09	0.05	-
		Coarse nitrate		0.09	0.1	0.08	0.13	-
		Total		0.2	0.15	0.17	0.18	0.14 [0.03, 0.42]
	Lifetime	Fine nitrate	days	6.2	7.2	3.7	5.6	-

		Coarse nitrate		2	2	4	4.2	-
		Total		3.2	2.7	3.9	4.6	5 [2, 7.8]
NH_3	Source	Emissions	Tg[N] yr^{-1}	53.5	53.5	53.6	50.5	51.8 [46.9, 58.1]
	Loss	Gas phase	Tg[N] yr^{-1}	-	-	-	0.6	-
		NH_4 formation		30.4	25.6	30.5	17.5	26.4 [18.4, 34.6]
		Dry deposition		17.4	20.4	12.7	21.3	15.4 [10.4, 24.1]
		Wet deposition		5.7	7.5	9.6	11.1	11 [5.6, 15.3]
		Total		53.4	53.5	53.6	50.5	53.2 [49.8, 57.9]
		Wet fraction	%	24.6	27	43	34.3	40.7 [24.5, 58.1]
	Burden		Tg[N]	0.04	0.06	0.07	0.09	0.16 [0.04, 0.7]
	Lifetime		days	0.28	0.41	0.46	0.63	0.72 [0.29, 0.98]
NH_4	Source	NH_3 conversion	Tg[N] yr^{-1}	30.4	25.6	30.5	17.5	23.7 [17.8, 29.5]
	Loss	Dry deposition	Tg[N] yr^{-1}	5.7	4.7	4.5	2.5	4.5 [1.3, 16.3]
		Wet deposition		24.9	21	25.9	14.9	20.7 [5.6, 34.6]
		Total		30.5	25.7	30.4	17.4	25.2 [17.7, 37.4]
		Wet fraction	%	81.4	81.8	85.2	85.6	81 [25.6, 94.7]
	Burden		Tg[N]	0.42	0.36	0.26	0.22	0.25 [0.13, 0.58]
	Lifetime		days	5	5	3.2	4.5	4.3 [1.9, 9.8]

Table 3: Global and annual-mean metrics for nitric acid (HNO_3), nitrate (NO_3), ammonia (NH_3) and ammonium (NH_4) in the FAST and SLOW simulations compared to Xu and Penner (2012) (XP12), Hauglustaine *et al.* (2014) (HA14) and the AeroCom phase III model intercomparison project described in Bian *et al.* (2017) (BI17). Square brackets in the BI17 column denoted the AeroCom inter-model range.

3.2 Annual mean burdens and concentrations

Figure 1 shows the annual-mean mass burdens of NH_4, fine NO_3 and coarse NO_3 in the FAST and SLOW simulations. While units of mg[N]m^{-2} are used in Fig. 1 and throughout the rest of the Results section, units of 'mg of substance per m^2' are used in the following text for direct comparison with HA14. Fine NO_3 associated with NH_4 is concentrated over land regions, particularly in the Northern Hemisphere. The fine NO_3 burden averaged over European land is 1 mg[NO_3]m^{-2} in SLOW and 3 mg[NO_3]m^{-2} in FAST. The total NO_3 burden over Europe is 3 mg[NO_3]m^{-2} in SLOW and 5 mg[NO_3]m^{-3} in FAST, which is close to the simulated present day values of 3-4 mg[NO_3]m^{-2} in HA14. Fine NO_3 peaks in Europe over the Mediterranean at 5 mg[NO_3]m^{-2} in SLOW and 12 mg[NO_3]m^{-2} in FAST. South Asia exhibits the greatest regional fine NO_3 burdens with 8 mg[NO_3]m^{-2} in SLOW and 14 mg[NO_3]m^{-2} in FAST. The total NO_3 burdens over South Asia of 11 mg[NO_3]m^{-2} in SLOW and 15 mg[NO_3]m^{-2} in FAST are somewhat greater than equivalent values in HA14 of 5-10 mg[NO_3]m^{-2}. Conversely, the total

NO_3 concentrations in East Asia (China) are smaller in these simulations (5 mg[NO_3]m^{-2} in SLOW and 9 mg[NO_3]m^{-2} in FAST) than in HA14 (10-20 mg[NO_3]m^{-2}). Over Central North America (the US), the total NO_3 burden is 2 mg[NO_3]m^{-2} in SLOW and 5 mg[NO_3]m^{-2} in FAST, which compares to 3-4 mg[NO_3]m^{-2} in HA14. In summary, the fine NO_3 concentrations are similar to the simulated present-day values in HA14 on a regional basis in FAST and SLOW. Of more importance to this study, FAST exhibits twice as much fine NO_3 burden on average as does SLOW in key industrialised land regions.

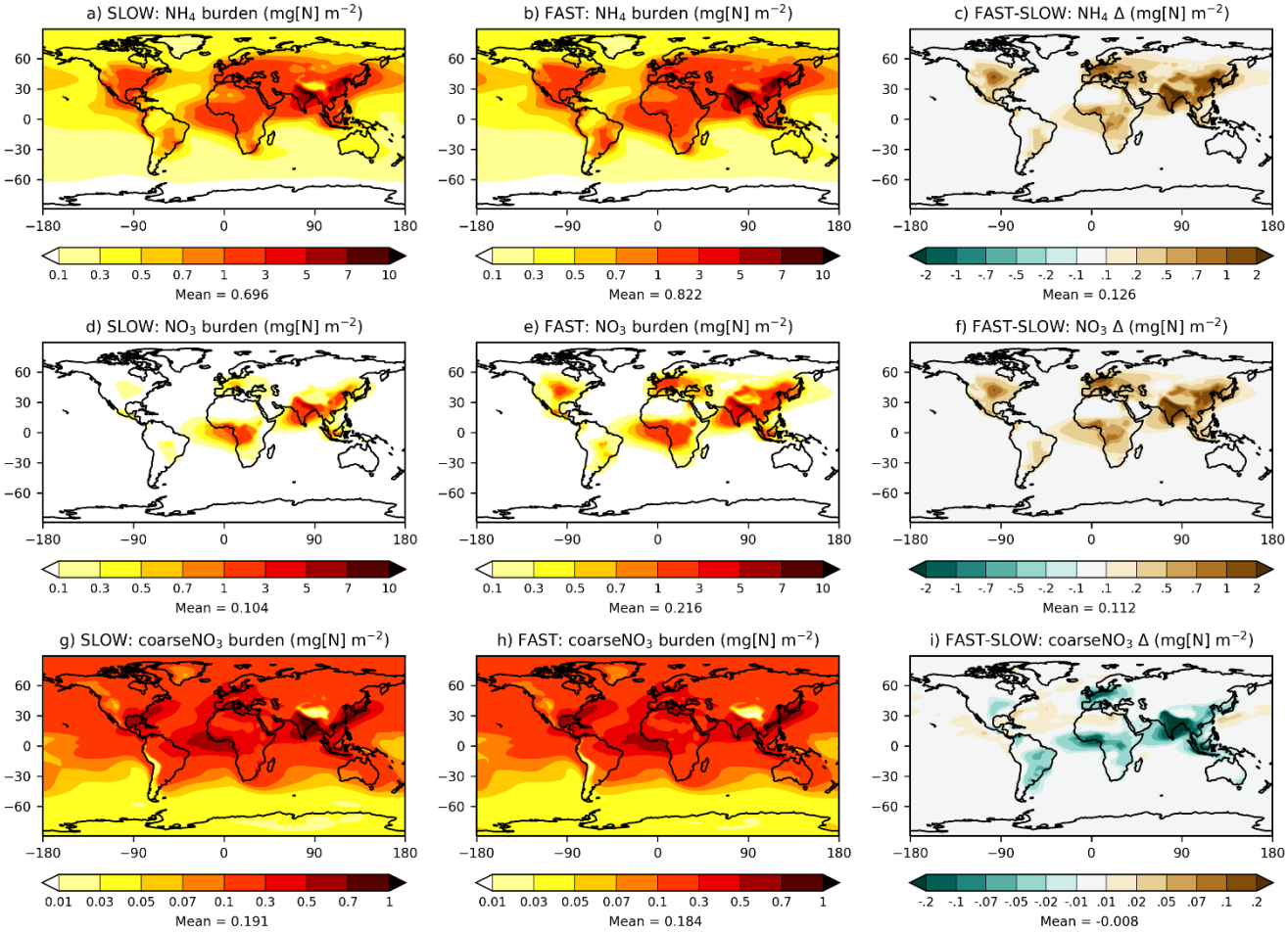

Figure 1: Annual-mean NH_4, NO_3, and coarseNO_3 burdens from the SLOW and FAST simulations

Whereas fine NO_3 burdens are concentrated over land, coarse NO_3 (i.e. coarseNO_3) is more evenly spread over the Earth and prevalent over maritime areas where it forms on sea-salt and aged dust particles (Figs 1g,h). Over European land, coarse NO_3

constitutes 31 % of the total NO_3 burden in FAST and 63 % in SLOW. Equivalent figures for East Asia are 15 and 30 %; South Asia – 10 and 23 %; and Eastern North America – 45 and 83 %. Therefore, the partitioning of NO_3 between the coarse and fine modes is highly sensitive to the uptake rate of HNO_3 on ambient aerosol (γ in Eq. 7).

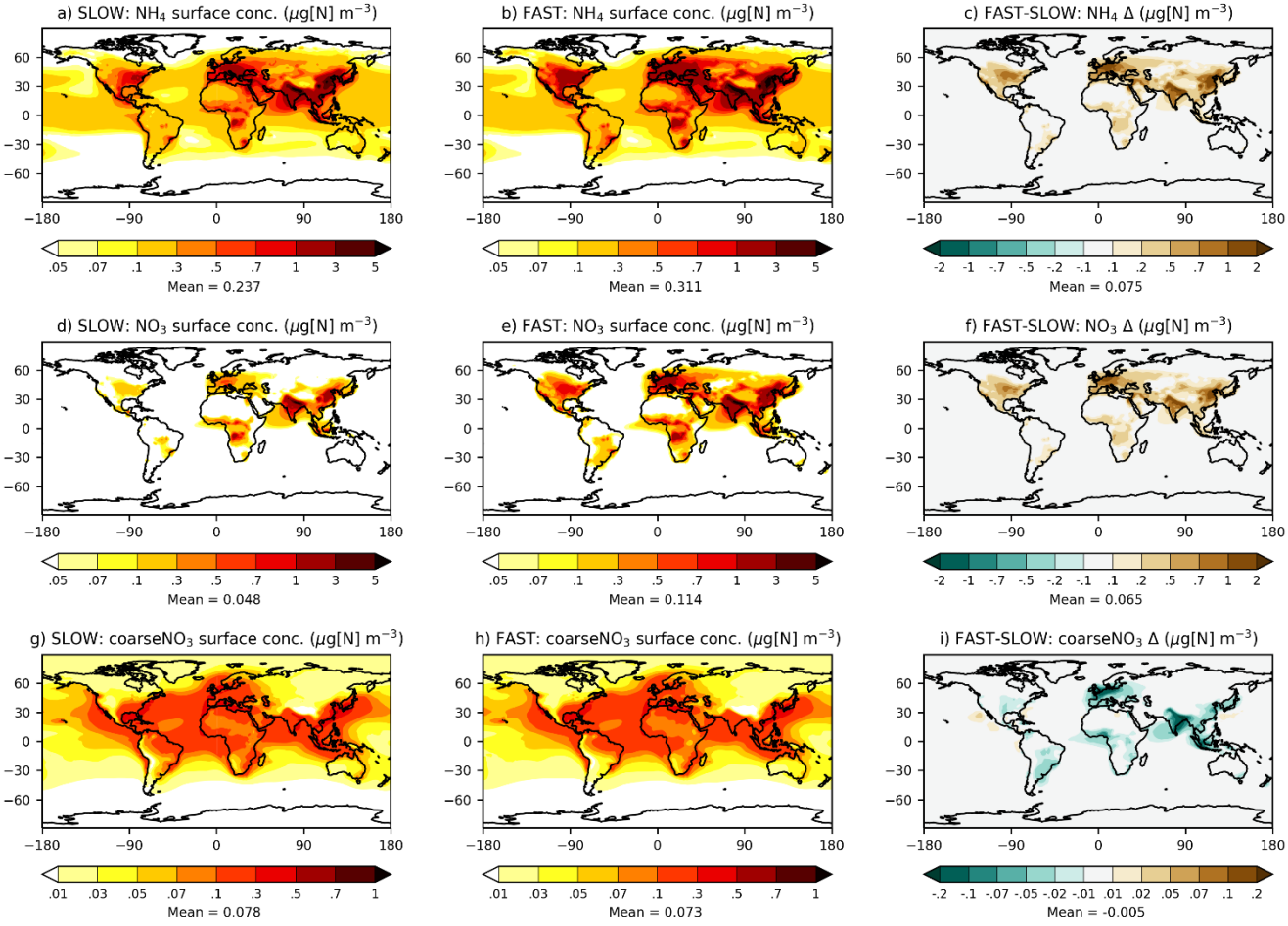

Figure 2: Annual-mean NH_4, NO_3, and coarseNO_3 near-surface concentrations from the SLOW and FAST simulations

Figure 2 shows maps of annual-mean near-surface concentrations of NH_4, fine NO_3 and coarse NO_3 in the SLOW and FAST simulations. The spatial distributions of fine NO_3 are similar to those reported in BI17 and HA14 with peak concentrations over North America, Europe, South Asia, South East Asia, and East Asia land regions, coincident with the highest NH_3 and NO_x emitting regions (Figure S6 in the Supplement). The average total NO_3 concentrations over Europe are 1.5 and 3.5 $\mu g[NO_3]m^{-3}$ in SLOW and FAST respectively, which can be compared to 4-5 $\mu g[NO_3]m^{-3}$ in HA14. Over Central North America, total NO_3 concentrations amount to 1 and 3 $\mu g[NO_3]m^{-3}$ on average in SLOW and FAST, with 50 % and 15 %

contributions from coarse NO_3. The regional-mean total NO_3 concentrations in East Asia amount to 3.5 and 6.5 $\mu g[NO_3]m^{-3}$ and in South Asia amount to 5.5 and 7.5 $\mu g[NO_3]m^{-3}$, in SLOW and FAST respectively. Total NO_3 differences between FAST and SLOW are driven by changes to the fine NO_3 concentrations (Figs 2d-f), with comparatively minimal changes to coarse NO_3 (Figs 2g-i). In summary, Fig. 2 shows that the near-surface NH_4NO_3 concentration differences between FAST and SLOW are very similar to the overall burden differences (Fig. 1).

Figure 3 shows the zonal mean, vertical distribution of NO_3, NH_4 and coarseNO_3 aerosol in the FAST and SLOW simulations. NH_4 reaches a greater altitude than fine NO_3 owing to its long-lived association with SO_4 aerosol (Figs 3a-b). Due to the high solubility of NH_3 gas and thus swift wet removal from the atmosphere, free ammonia is mostly limited to the bottom 1 km of the atmosphere (Bellouin *et al*., 2011), which limits the vertical extent to which $NH_4{\cdot}NO_3$ may form by condensation (Figs 3c-d). This is further corroborated by Figure S7 in the Supplement which shows the 'gas ratio', defined as $([NH_3] + [NH_4] - 2 \times [SO_4])$ divided by $([HNO_3] + [NO_3])$, with values greater than 1 indicating that conditions are HNO_3-limited and less than 1 indicating conditions are NH_3-limited (Ansari and Pandis, 1998). It is clear from Fig. S7 that $NH_4{\cdot}NO_3$ production is HNO_3-limited at the surface over land regions but that conditions are ubiquitously NH_3-limited above altitudes of 1000 m. While $NaNO_3$ and $Ca(NO_3)_2$ are not volatile like $NH_4{\cdot}NO_3$, they are instead associated with coarse particles that are readily removed from the atmosphere by gravitational sedimentation and wet scavenging, and thus remain confined to the lowest 1 km of the atmosphere (Figs 3e-f). Figure 3 demonstrates that NH_4NO_3 and coarseNO_3 are mostly confined to the lower troposphere in the UM in agreement with other GCMs.

3.3 Regional surface concentrations

Given the strong dependency of the ammonia-nitrate equilibrium on temperature, and the pronounced seasonal cycle in precursor gas emissions, it is important to consider the seasonal cycle of NO_3 when assessing a nitrate scheme. Figure 4 shows the seasonal cycles in NO_3, and coarseNO_3 near-surface concentrations and associated regional NH_3 emissions averaged over land in 9 'Giorgi' regions (Giorgi, 2006), selected due to their high fine NO_3 concentrations (Fig. 2). Table S6 in the Supplement gives details of the 'Giorgi' regions. For most of the regions (NEU, MED, CNA, EAS, WAF, SQF, and to a lesser extent SEA), fine NO_3 cycles in both the FAST and SLOW simulations are tightly coupled to cycles in regional NH_3 emissions, which further corroborates the notion that $NH_4{\cdot}NO_3$ formation may be limited in these regions by available NH_3. $NH_4{\cdot}NO_3$ concentrations in the CAS and SAS regions may be more dependent on seasonal meteorology than other regions, for instance SAS (i.e. South Asia) experiences a strong summer monsoon which would enhance wet deposition of $NH_4{\cdot}NO_3$ during summer and thus reduce concentrations in contrast to the high NH_3 emissions in this period. SAS also has consistently elevated NH_3 emissions throughout the year and is thus less sensitive to seasonal cycles in NH_3 emissions (Zhu *et al*., 2015). In all regions, NH_4 and fine NO_3 concentrations exhibit a strong seasonal cycle in both SLOW and FAST while the seasonal cycle in coarse NO_3 is less apparent. In the SLOW simulation, coarse NO_3 concentrations are of similar magnitude to fine NO_3 concentrations in NEU, MED, CAS, CNA, and WAF on a regional-mean basis (Fig. 4). In summary, Fig. 4 shows the tight coupling between

regional NH_3 emissions and adjacent NO_3 surface concentrations in many regions and highlights the strong seasonality of NH_4NO_3 in the UM.

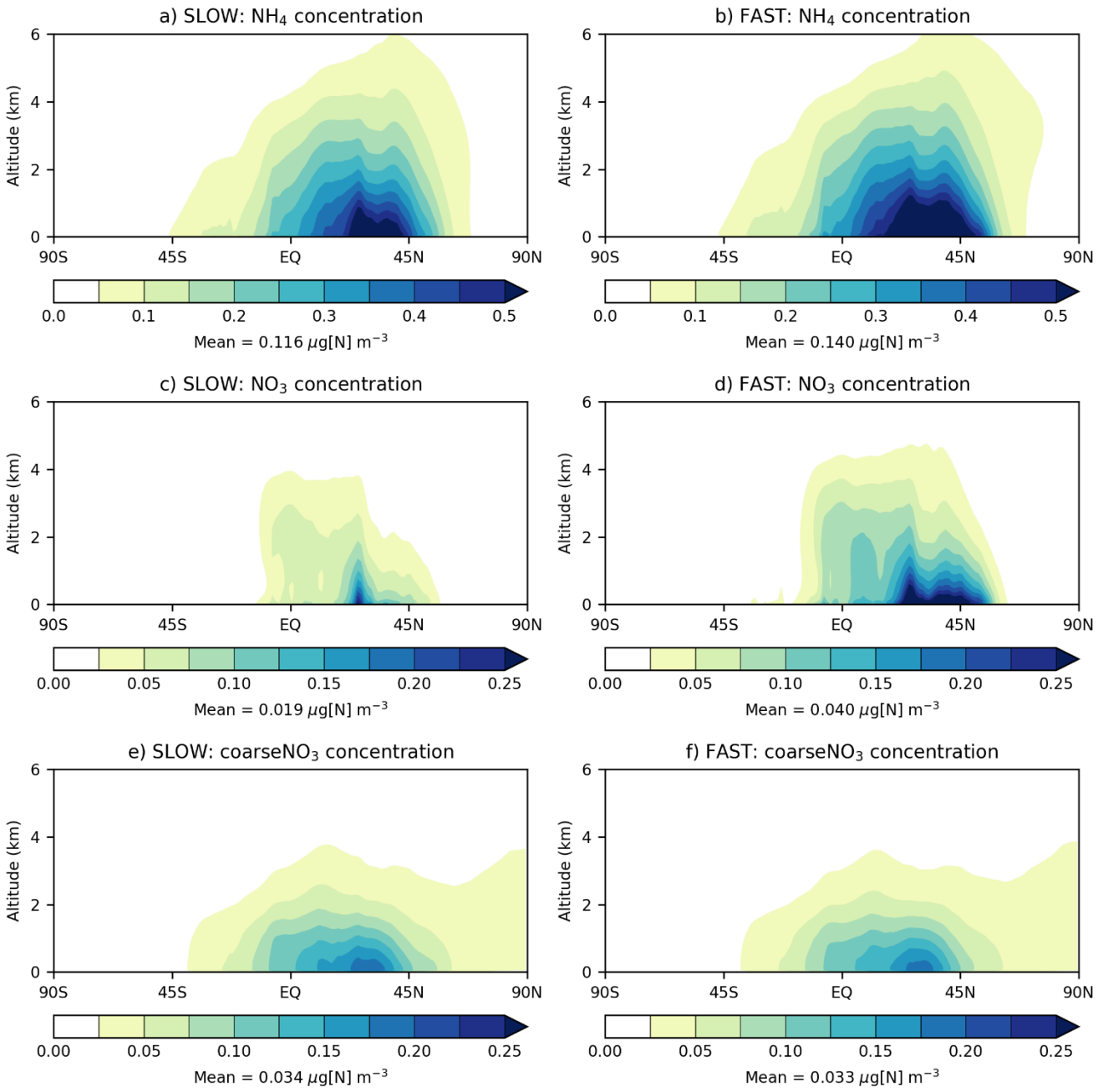

Figure 3: Annual and zonal-mean NH_4, NO_3, and coarseNO_3 concentrations vs altitude from the SLOW and FAST simulations

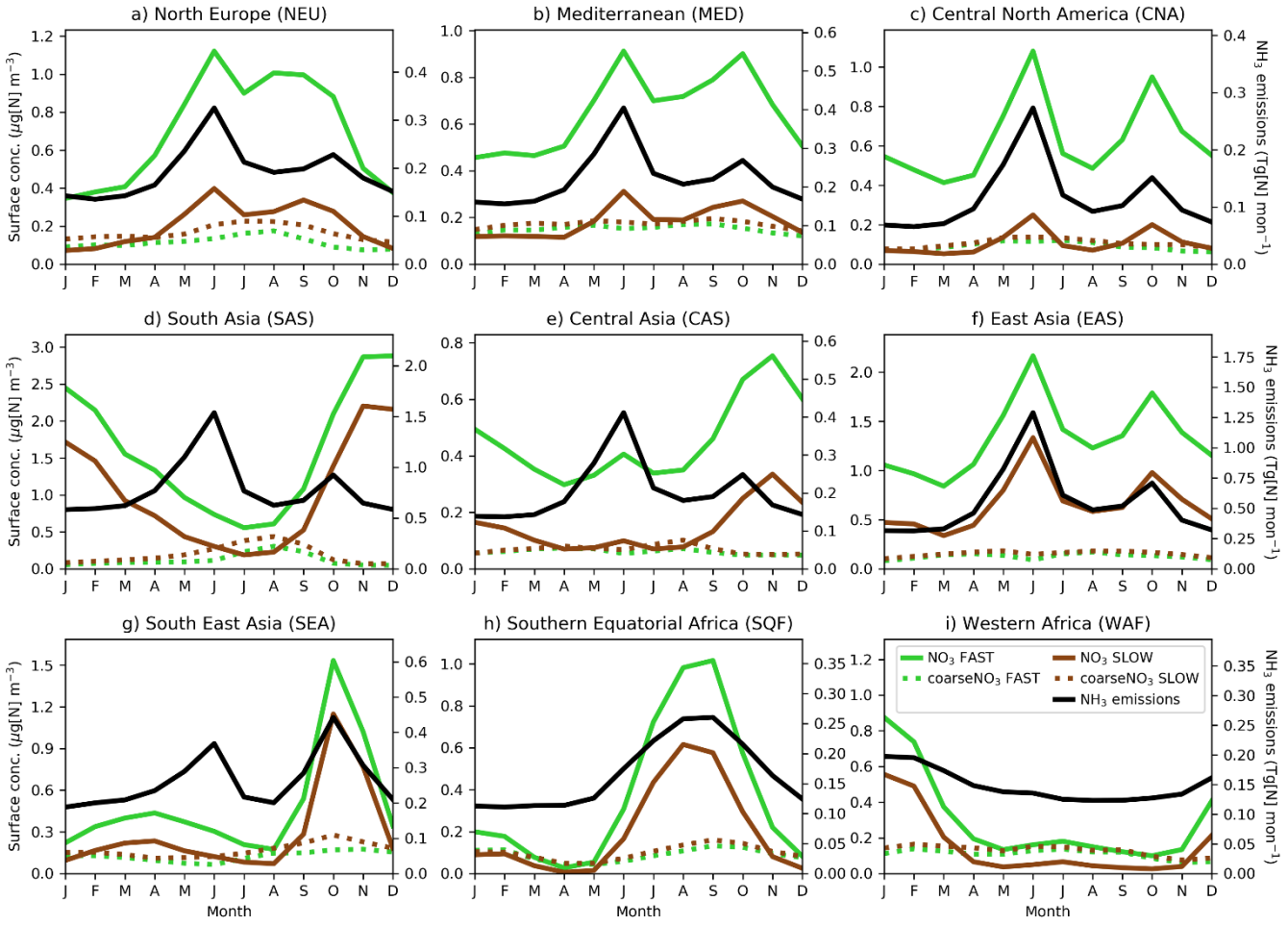

Figure 4: Regional and monthly-mean NO_3 (solid line) and coarseNO_3 (dashed line) near-surface concentrations and NH_3 emissions (solid black line) time-series for the SLOW (brown) and FAST (green) simulations for 9 'Giorgi regions' [Giorgi, 2006] (land-only) representing areas with high NO_3 concentrations.

When introducing an aerosol such as NH_4NO_3 to a GCM, it is essential to validate the model by comparing the simulated concentrations to observations. Figures 5 and 6 show the near-surface concentrations of HNO_3, NH_4 and total NO_3 over the US (Fig. 5) and Europe (Fig. 6) in the FAST and SLOW simulations compared to observations from the Clean Air Status and Trends Network (CASTNet, www.epa.gov/castnet, last access: January 2021, Finkelstein *et al.* (2000)) for the US and the European Monitoring and Evaluation Programme (EMEP, http://ebas.nilu.no/, last access: March 2021, Torseth *et al.* (2012)) for Europe. In both networks the sites are located so as to represent the wider region. Data processing and site selection for the observations follows the methodology described in Hardacre *et al.* (2021), who have compared SO_2 and SO_4 concentrations

from UKESM simulations with CASTNet and EMEP observations. CASTNet and EMEP data are averaged over the period 1994-2013 where available. For CASTNet there are a total of 49 sites that meet data processing criteria in this study. For EMEP there are 59 sites for HNO_3, 59 sites for NH_4 and 80 sites for NO_3 meeting data processing criteria over the 1994-2013 timeframe. For the scatterplots in Figs 5 and 6, model output is interpolated to measurement sites using a nearest-neighbour approach assuming the Earth is a sphere. It is important to note that the absolute magnitudes of concentrations are not directly comparable between the simulations and observations given that the simulations assume constant NO_x and NH_3 emissions based on the year 2000 whereas NO_x and NH_3 emissions in reality are transient. This becomes apparent when comparing the network-mean concentrations in the simulations with the observations (Figure S8 in the Supplement) where there is a clear negative trend in HNO_3, NH_4 and NO_3 concentrations in both CASTNet and EMEP observations from 1994 to 2013.

Figure 5 shows that the spatial distributions of HNO_3, NO_3 and NH_4 over the US are similar in FAST and SLOW, with peak HNO_3 concentrations in the east and midwestern states reflecting industrial NO_x emissions, and peak NO_3 and NH_4 in the midwestern and central states reflecting agricultural NH_3 emissions (Park *et al*., 2004). The absolute magnitudes of NH_4 and NO_3 concentrations are closer to CASTNet observations in SLOW (Fig. 5h) than in FAST (Fig. 5i), but the spatial correlation coefficient for NO_3 is better in FAST (R = 0.69) than in SLOW (R = 0.43). This suggests that the positive NO_3 (and correspondingly NH_4) biases in FAST may partially emanate from a surplus of HNO_3 in the model, given that HNO_3 is positively biased in both FAST and, to an even greater extent, SLOW (Fig. 5d). Because of the underlying HNO_3 bias, it is not possible to declare whether FAST or SLOW is the better model from comparison with the CASTNET observations (Fig. 5). It is only possible to deduce that reducing the HNO_3 uptake coefficient (γ) in SLOW leads to a substantial reduction in total NO_3 concentration, as already shown in Figs 1, 2 and 4.

Over Europe, NO_3 and NH_4 concentrations are closer to EMEP observations in the SLOW simulation than in the FAST simulation (e.g. smaller mean biases in Figs 6d,g). NO_3 concentrations in both FAST and SLOW peak in the Po Valley (North Italy) and Benelux Region (Belgium and the Netherlands), in anecdotal concordance with Druge *et al*. (2019) and references therein. The Po Valley peak in both the EMEP observations and simulations is due to the entrapment of industrial air pollution by regional geography. The observed NH_4 and HNO_3 peaks over the Czech Republic may be attributable to high agricultural NH_3 emissions pre-2004, with concomitant concentration declines owing to the Gothenburg protocol (Fortems-Cheiney *et al*., 2016; Giannakis *et al*., 2019). Neither of the observed NH_4 or HNO_3 concentration peaks in the Po Valley or the Czech Republic are well captured by FAST or SLOW simulations which may be attributed to the coarse model resolution employed here (N96) and the close proximity of measurement sites to NH_3 sources. In summary, Figs 5 and 6 demonstrate the high skill of the UM nitrate scheme in capturing the magnitude of observed HNO_3, NH_4 and NO_3 concentrations and highlight how the HNO_3 uptake coefficient (γ) could be used to tune NH_4 and NO_3 concentrations in a GCM to observations.

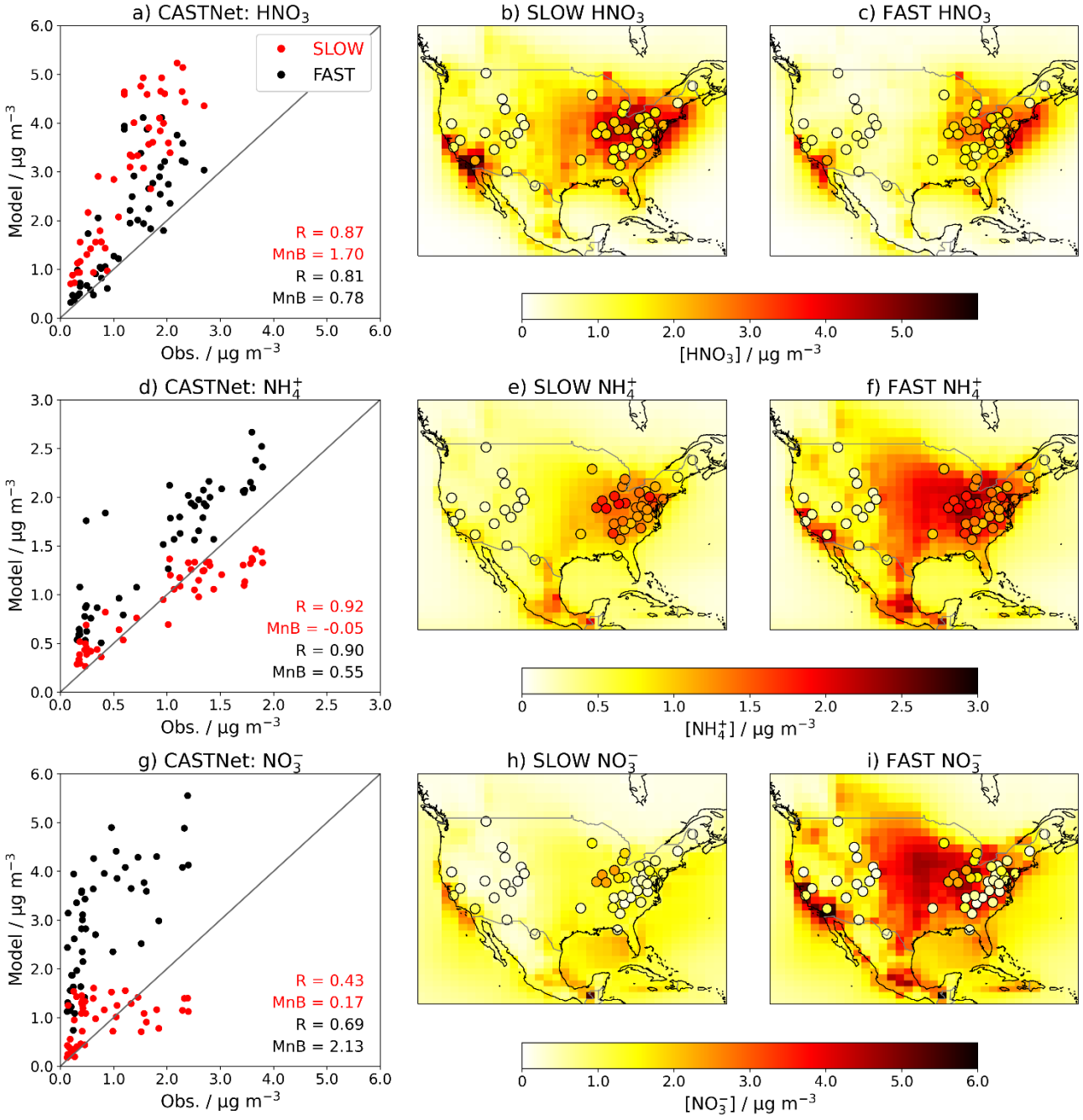

565

Figure 5: Annual-mean HNO_3, NH_4 and total-NO_3 near-surface concentrations in the FAST and SLOW simulations over North America compared to CASTNet observations averaged over 1994-2013. In (b), (c), (e), (f), (h) and (i), coloured contours show simulated concentrations while overlayed filled circles represent CASTNet observations. In (a), (d), and (g), 'R' is the Pearson's correlation coefficient and 'MnB' is the mean bias between simulated and observed concentrations

570

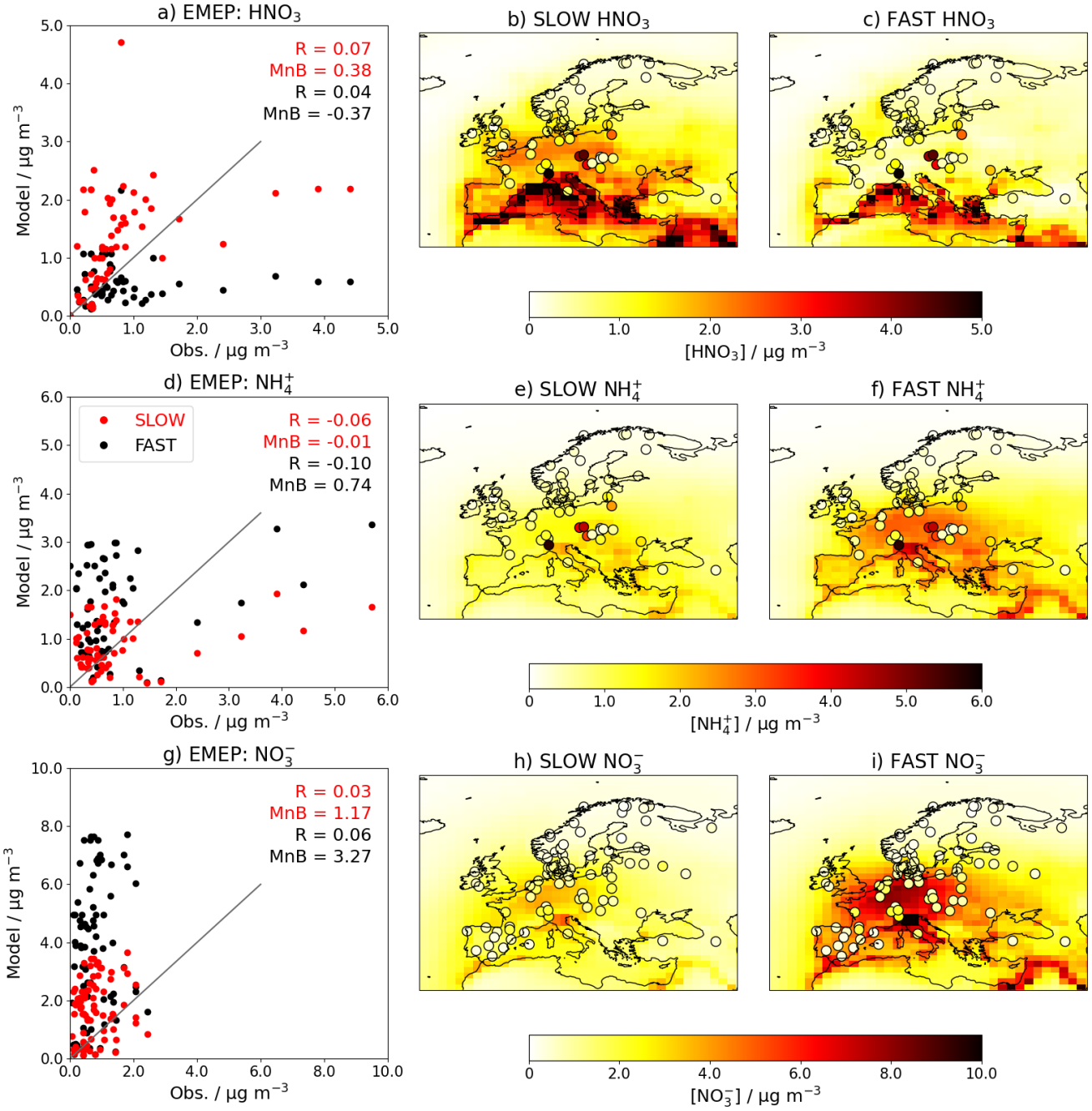

Figure 6: Annual-mean HNO_3, NH_4 and total-NO_3 near-surface concentrations for the FAST and SLOW simulations over Europe compared to EMEP observations averaged over 1994-2013 where available. In (b), (c), (e), (f), (h) and (i), coloured contours show simulated concentrations while overlayed filled circles represent EMEP observations. In (a), (d), and (g), 'R' is the Pearson's correlation coefficient and 'MnB' is the mean bias between simulated and observed concentrations

Given that NH_4NO_3 has a strong diurnal tendency, it is important to compare the simulated diurnal concentrations from the UM with observations, particularly if the scheme is to garner further utility by contributing to air quality forecasts in the future. Figure 7 shows the statistical distribution of 6 hourly total NO_3 and NH_4 concentrations from the FAST and SLOW simulations (years 2004-2013) interpolated to two EMEP supersites in the UK – Auchencorth Moss and Chilbolton Observatory – and compared with observed diurnal concentrations from those sites (UK AIR, https://uk-air.defra.gov.uk/data/, last access: 29 January 2021). Both sites use MARGA instruments – a combination of wet rotating denuders for gas measurements, and stream jet aerosol collectors for aerosol measurements – allowing for accurate partitioning between the aerosol and gas phases for volatile ammonium nitrate (Aas *et al*., 2012; Twigg *et al*., 2016). Only data recorded at the precise hours of 06:00, 12:00, 18:00, and 24:00 UTC that has passed the Department for Environment, Food & Rural Affairs' **(**DEFRA) quality control is utilised from the observations. Figure S9 in the Supplement shows the equivalent statistics for HNO_3 and NH_3 gases compared to observations. It is clear from Fig. 7 that NH_4 and NO_3 are significantly reduced in the SLOW simulation with respect to the FAST simulation in both seasons. It is also clear that the diurnal cycle, with NH_4 and NO_3 peaking at night (24Z or 00Z) and early morning (06Z) is both observed and skilfully simulated in both FAST and SLOW. Interestingly, the model shows similar biases to the Met Office's AQUM in: an over prediction of NO_3 during night-time in the summer; a slight under prediction of NO_3 in the winter; a large over prediction of HNO_3 during the day in the summer; and a smaller over-prediction of HNO_3 at night in the winter. The curious over-prediction of NH_3 at night in winter (Fig. S9 in the Supplement) was also observed in previous incarnations of the AQUM and will be addressed in the UM in future by imposing a diurnal cycle to NH_3 emissions. In summary, the pronounced diurnal NH_4NO_3 cycle from UK AIR observations is generally well captured by the UM nitrate scheme (Fig. 7).

As NH_4NO_3 is a significant contributor to urban air pollution episodes (Jiminez *et al*., 2009), it is important to assess the contribution of NH_4NO_3 to overall $PM_{2.5}$ surface concentrations using observations for validation. Figure 8 shows the seasonal cycle in total $PM_{2.5}$ concentrations in the CNTL, FAST, and SLOW simulations compared to collocated $PM_{2.5}$ observations from the Global Aerosol Synthesis and Science Project (GASSP; http://gassp.org.uk/data/, last access: 2 July 2020, Reddington *et al.*, 2017). GASSP amalgamates non-urban $PM_{2.5}$ measurements from three major networks: The Interagency Monitoring of Protected Visual Environments (IMPROVE) project in North America, the European Monitoring and Evaluation Programme (EMEP), and Asia-Pacific Aerosol Database (A-PAD). The $PM_{2.5}$ analysis proceeds as in Turnock *et al.* (2020), with monthly-mean observations determined for each measurement site averaged over the years 2000-2010 and over each region. This is then compared with the simulated $PM_{2.5}$ output that has been interpolated to individual site locations using a nearest-neighbour approach and averaged over the same time period and regions. Also shown in Fig. 8 is Modern-Era Retrospective Analysis for Research and Applications, version 2 (MERRA-2) reanalysis data (Buchard *et al.*, 2017; Randles *et al.*, 2017), which closely follows GASSP surface observations in Europe and North America but is less successful in other

regions where a smaller number of ground-based observations are available, for example, incorrectly modelling the seasonal $PM_{2.5}$ cycles in South Asia and Pacific AUS NZ.

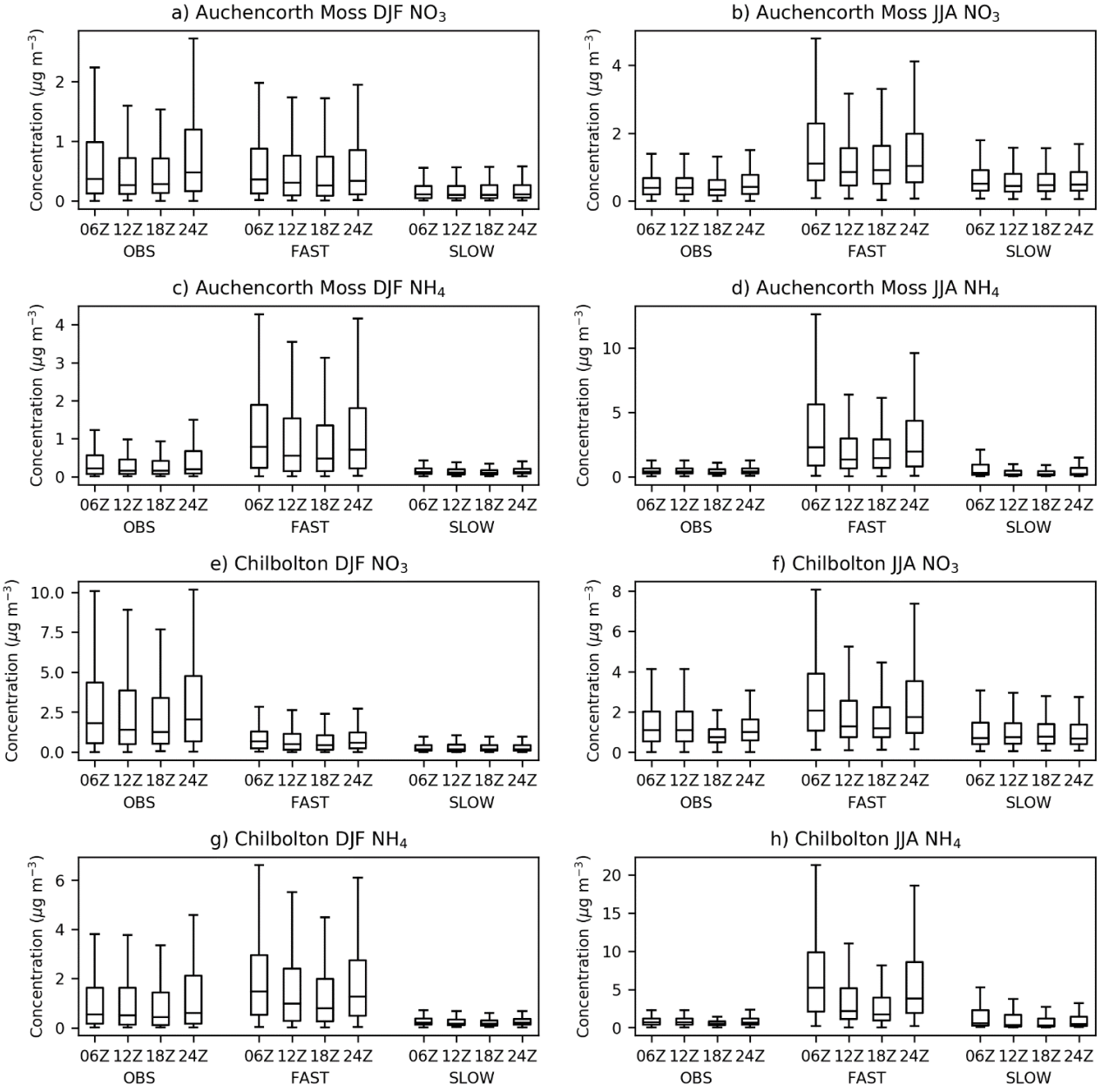

615 **Figure 7: December-February (DJF) and June-August (JJA) diurnal cycles of near-surface total-NO_3 and NH_4 aerosol concentrations in the FAST and SLOW simulations interpolated to two European Monitoring and Evaluation Programme (EMEP) supersites in the UK – Auchencorth Moss [55.79216ºN, -3.2429ºE] and Chilbolton [51.149617ºN, -1.438228ºE], alongside 6 hourly observations from 2014-2018 for Auchencorth Moss and 2016-2020 for Chilbolton**

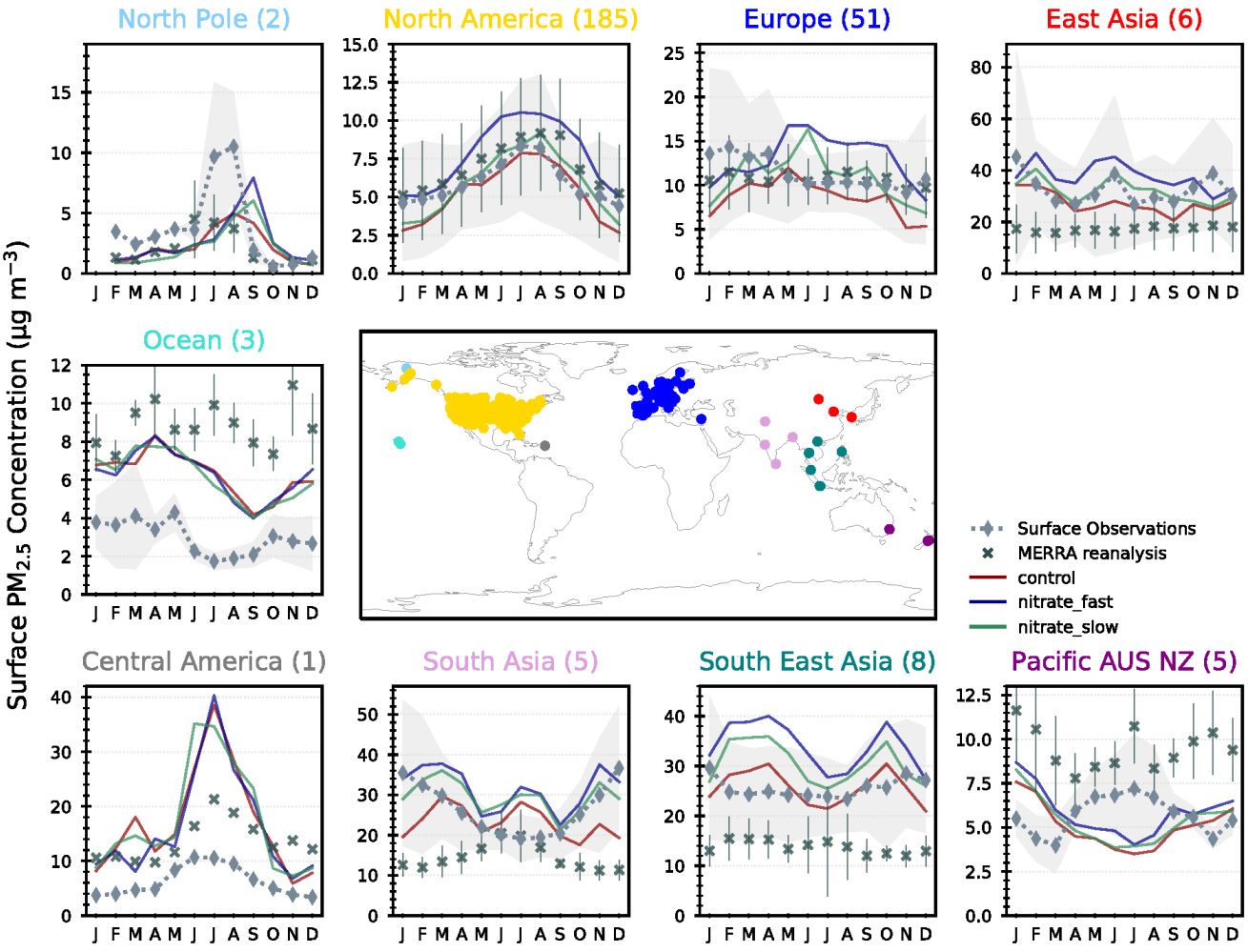

620 **Figure 8: Regional and monthly-mean surface $PM_{2.5}$ concentrations in the UM simulations (CNTL=red, FAST=blue, and SLOW=green lines), and from MERRA reanalyses and GASSP surface observations**

Over North America, the slight negative $PM_{2.5}$ bias in CNTL is brought closer to observations in SLOW and over-corrected in FAST which now exhibits a slight positive bias (Fig. 8). Over Europe observations suggest that $PM_{2.5}$ slightly peaks in DJF, 625 which is not the case in any of the UM simulations in which $PM_{2.5}$ peaks in JJA. Druge *et al.* (2019) observed the same seasonal bias over Europe in the ALADIN-Climate regional model, which they attributed to uncertainties in the annual cycle of NH_3 and HNO_3 precursor gases. In Fig. 7, the simulated NH_4 concentrations in JJA vastly exceeded the observations at both UK-based supersites, indicating that summertime NH_3 gas emissions may be biased high in the prescribed CEDS emissions dataset over Europe. Another source of uncertainty that may affect the seasonal NH_4NO_3 cycles is the dependence of heterogeneous 630 N_2O_5 hydrolysis on relative humidity and aerosol liquid water content. In the UM, N_2O_5 hydrolysis on sulphate is modelled using a fixed uptake coefficient of 0.1, whereas Shah *et al.* (2018) have shown that a humidity and acidity dependent uptake

coefficient improves $PM_{2.5}$ forecasts in winter over the eastern US. This suggests that differences in the seasonal cycles of NH_4 and NO_3 may emanate from imprecisions in the modelling of precursor gas emissions, chemistry, and deposition (Bian *et al.*, 2017).

Returning to Fig. 8, over South Asia, East Asia, and South East Asia the CNTL simulation adeptly captures the seasonal $PM_{2.5}$ cycle and the addition of NH_4NO_3 in FAST and SLOW induces a slight positive bias. In summary, Fig. 8 demonstrates that both SLOW and FAST have a significant impact on overall $PM_{2.5}$ concentrations – particularly over Europe, Asia, and North America – with FAST inducing approximately double the $PM_{2.5}$ increase than in SLOW. The addition of NO_3 to the UM may help to reduce the long standing $PM_{2.5}$ biases in North America and Europe. Additionally, Fig. 8 provides further evidence that NH_3 emissions over Europe in the CEDS emissions dataset may be biased high during the summer.

3.4 Aerosol optical depth and radiation changes

Atmospheric NH_4NO_3 aerosol may have significant radiative implications on a regional basis leading to climate changes (Hauglustaine *et al.*, 2014). It is thus useful to compare the aerosol optical depth and Top-Of-the-Atmosphere (TOA) radiative flux changes in the FAST and SLOW simulations with CNTL to estimate the radiative impact of NH_4NO_3. Figure 9 shows the annual-mean total aerosol optical depth at 550 nm (AOD_{550}) in the UM simulations (CNTL, FAST, and SLOW), with contributions from the Aitken, accumulation and coarse soluble modes, the Aitken insoluble mode, and mineral dust. Also plotted is the 2003-2012 mean MODIS 'collection 6' AOD_{550} satellite data, which merges NASA's "Dark Target" and "Deep Blue" algorithms and is widely used for validating aerosol models (Levy *et al*., 2013; Hsu *et al*., 2013). The MODIS AOD_{550} is included in Fig. 9 to assess the skill of the CNTL simulation at capturing the observed AOD_{550} distribution. It is clear that generally the CNTL simulation does a reasonable job of simulating the spatial distribution of AOD_{550} (Fig. 9a) when compared to MODIS (Fig. 9d).

The new nitrate scheme will impact the total AOD_{550} by various direct and indirect routes. Firstly, the addition of NO_3, NH_4 and coarseNO_3 mass will increase the size and change the composition of the ambient aerosols thus altering their optical properties. Secondly, coarseNO_3 mass associated with sea-salt will replace existing NaCl thus changing the aerosol composition. Thirdly, the explicit addition of NH_4 to the hygroscopic growth routine will reduce hygroscopic growth, whereas NO_3 and coarseNO_3 will promote hygroscopic growth. Finally, tropospheric SO_4 was previously assumed to uniformly take the form of $(NH_4)_2SO_4$ in terms of optical properties, but in the new nitrate scheme is explicitly divided into H_2SO_4 and $(NH_4)_2SO_4$ contributions based on NH_4 abundance. Indirectly, NH_4 and NO_3 may alter the AOD_{550} by impacting online aerosol emissions (such as dust and sea-salt) and atmospheric oxidant concentrations in the UM.

The AOD_{550} differences between the CNTL and nitrate simulations (FAST and SLOW) shown in Fig. 9 are a combination of the various direct and indirect changes to the UM listed above which do not necessarily result in an increase to AOD_{550}. The global-mean AOD_{550} difference between FAST and CNTL of +0.0048 is serendipitously close to equivalent nitrate AODs in the literature such as +0.006 in Paulot *et al.* (2016), +0.005 in HA14, and +0.006 [+0.002, +0.009] in Myhre *et al.* (2013), although it is important to note that the AOD_{550} changes in those studies were derived from difference between present-day (PD) and pre-industrial (PI) simulations, rather than PD with and without nitrate. This is a subtle but important difference which reduces comparability given that the PI simulations included nitrate, albeit at much smaller concentrations than in PD (Hauglustaine *et al.*, 2014). Despite the negligible global AOD_{550} difference between FAST and CNTL, there are significant regional perturbations such as +0.05 over Northern Europe as a whole, +0.08 over East Asia, +0.19 over South Asia, and +0.04 over West Africa and Southern Equatorial Africa (Fig. 9c). The changes in the SLOW simulation are more subtle, for instance, AOD_{550} changes by -0.007 over Northern Europe, +0.013 over East Asia, +0.1 over South Asia, and +0.018 over West Africa and Southern Equatorial Africa (Fig. 9f).

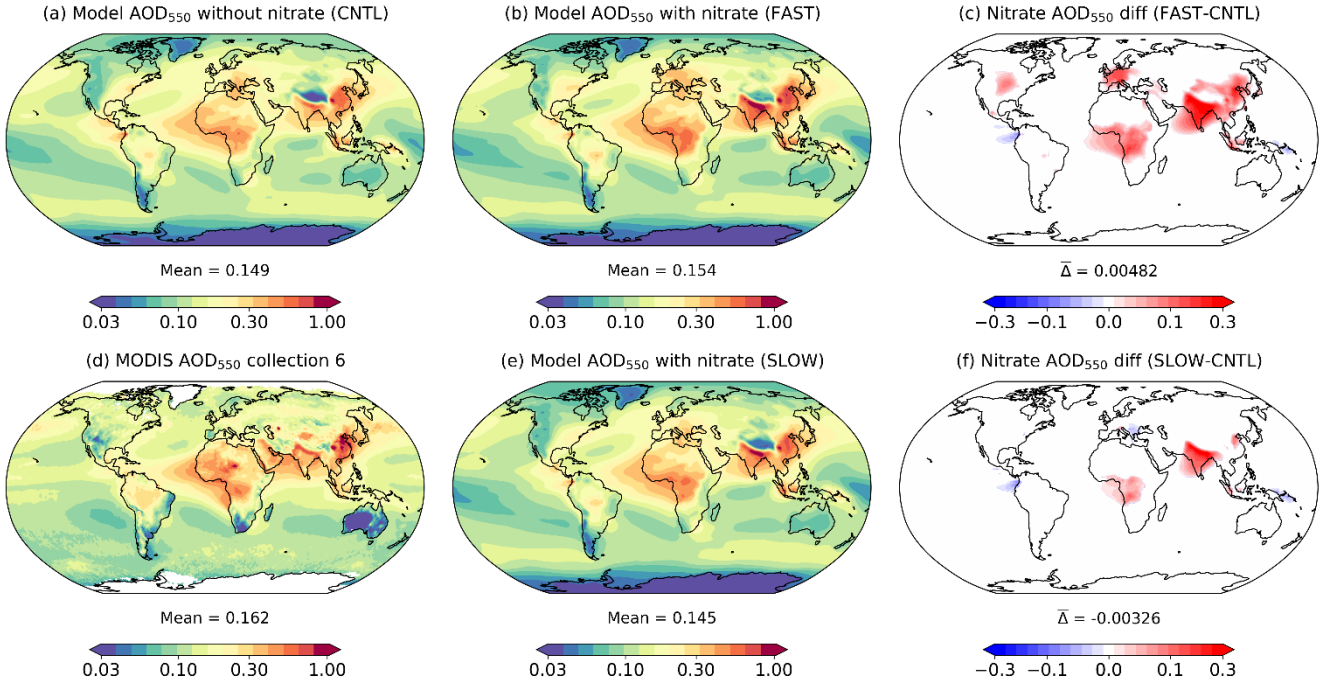

Figure 9: Annual-mean and column-integrated 550nm aerosol optical depth (AOD_{550}) in the CNTL, FAST, and SLOW simulations and from MODIS collection 6 satellite observations. (c) and (f) show the difference between the FAST and CNTL, and SLOW and CNTL, simulations respectively

Figure S10 in the Supplement shows the annual-mean all-sky radiative flux perturbation at the TOA. As the UM simulations are atmosphere-only with fixed sea-surface temperatures and sea-ice fields, the TOA radiative flux perturbation can also be

denoted the total Effective Radiative Forcing (ERF) (Bellouin *et al*., 2020). The global-mean ERFs from FAST-CNTL and SLOW-CNTL are -0.19 Wm^{-2} and -0.07 Wm^{-2} respectively, which is a similar magnitude to the PD-PI nitrate RFs of -0.056 Wm^{-2} in HA14, -0.17 Wm^{-2} in Bellouin *et al*. (2011), and -0.08 [-0.02, -0.12] Wm^{-2} in Myhre *et al*. (2013), although note again that the RFs in those studies were derived from difference between present-day (PD) and pre-industrial (PI) simulations, rather than PD with and without nitrate, and those studies determined the direct radiative forcing rather than the total ERF which also includes indirect radiative impacts of cloud and atmospheric composition changes. An explicit assessment of nitrate-induced changes to cloud properties is outside the scope of this study. Although most regions exhibit insignificant radiative differences between FAST and CNTL in Fig. S10b (where stippling indicates significant changes at the ±2σ level), there are significant changes over Europe (min = -3.7 Wm^{-2}, mean = -1.5 Wm^{-2}), South Asia (min = -10.3 Wm^{-2}, mean = -3.2 Wm^{-2}), and Southern Equatorial Africa (min = -3.8 Wm^{-2}, mean = -1.2 Wm^{-2}). This mirrors nitrate's radiative signal in HA14. The SLOW simulation exhibits smaller radiative impacts than FAST, with significant changes limited to South Asia (min = -7.7 Wm^{-2}, mean = -1.5 Wm^{-2}) and Southern Equatorial Africa (min = -3.5 Wm^{-2}, mean = -0.7 Wm^{-2}). Figures 9 and S10 highlight the regionality of ammonium nitrate climate forcing and further demonstrate the significant differences between the FAST and SLOW simulations.

4 Conclusions and Discussion

A thermodynamic equilibrium nitrate scheme has been added to UKCA-mode and tested in the Met Office's Unified Model. In contrast to widely utilised 'instantaneous' thermodynamic equilibrium models, the UKCA nitrate scheme limits the rate at which ammonium nitrate (NH_4NO_3) concentrations reach equilibrium using first-order condensation theory. Sensitivity tests are performed to assess the sensitivity of NH_4NO_3 concentrations to the nitric acid (HNO_3) uptake coefficient (γ in Eq. 7). Specifically, two values of γ are chosen to represent fast uptake rates ($\gamma = 0.193$; FAST) and slow uptake rates ($\gamma = 0.001$; SLOW) based on the range of γ measurements from the literature (e.g. Bauer *et al*., 2004). While it is known that γ varies with aerosol composition, temperature, and relativity humidity (e.g. Vlasenko *et al*., 2006), well-constrained values for HNO_3 uptake on common aerosol species (e.g. sulphate, organic carbon, black carbon) are at present lacking. As a first order sensitivity test, the HNO_3 uptake coefficient used in NH_4NO_3 production is assumed to be globally invariant to aerosol composition (with the exception of mineral dust), temperature and relative humidity in FAST and SLOW. A third nitrate simulation in which NH_4NO_3 reaches thermodynamic equilibrium instantaneously (INSTANT), is shown to produce near-identical results to FAST. This is the first study to investigate the sensitivity of NH_4NO_3 concentrations to the HNO_3 uptake coefficient and provide an efficient method for reducing NO_3 concentration biases in GCMs.

To help evaluate the sensitivity of NH_4NO_3 concentrations to HNO_3 uptake coefficient, and the suitability of the FAST and SLOW uptake coefficients, a range of surface and satellite observations and comparable modelling studies have been compared to the UM simulations. Many robust results emerge from the simulations. Fine NO_3 concentrations are a factor of 2 greater in

FAST than in SLOW on a global-mean basis, with associated increases to NH_4 concentrations in FAST. The largest differences are over land regions in North America, Europe, South and East Asia, and Equatorial Africa. However, there are minimal differences between coarse NO_3 (associated with dust and sea-salt) concentrations in FAST and SLOW. Over many populous land regions (Europe, North America, East and South East Asia, and West and Equatorial Africa), seasonal near-surface $NH_4{\cdot}NO_3$ concentrations are closely correlated with seasonal NH_3 emissions suggesting that NH_3 availability is the limiting factor controlling $NH_4{\cdot}NO_3$ prevalence (Giannakis *et al.*, 2019). In the SLOW simulation, coarse NO_3 concentrations are of a similar magnitude to fine NO_3 concentrations over many industrialised regions. Comparing the simulated concentrations to CASTNet observations (i.e. the US network), FAST better captures the spatial distribution of near-surface NO_3, NH_4, and HNO_3 concentrations but is positively biased, whereas SLOW better captures the magnitude of the concentrations. Total NO_3 concentrations over Europe are comparable between SLOW and EMEP observations but are a factor of 3-4 too high in FAST. Many of the biases in simulated NH_4 and NO_3 concentrations appear to be artefacts of biases in precursor gas (HNO_3 and NH_3) concentrations. Significant AOD and TOA radiative flux impacts are mostly isolated to land regions with substantial $NH_4{\cdot}NO_3$ burdens. On a global mean basis, the nitrate ERF is -0.17 Wm^{-2} in FAST and -0.07 Wm^{-2} in SLOW which mirrors the ratio of $NH_4{\cdot}NO_3$ burdens in the two simulations.

Introducing a kinetic limitation on the rate at which $NH_4{\cdot}NO_3$ concentrations reach equilibrium has minimal effect for γ = 0.193 (i.e. comparing FAST with INSTANT) but a significant effect equivalent to a halving for γ = 0.001 (i.e. comparing SLOW with FAST). In general, FAST exhibits better spatial correlation with observed nitrate surface concentrations while SLOW better resolves the magnitude of surface concentrations. Note though that there are many caveats associated with this study. Using a globally uniform value for the HNO_3 uptake coefficient (γ) obviates the dependence of γ on aerosol composition and relative humidity. A better parameterisation may instead utilise a volume-weighted γ depending on aerosol composition and ambient relative humidity. Additionally, assuming the same value of γ for both HNO_3 and NH_3 is a pragmatic simplification owing to the dearth of γ measurements. For example, Benduhn *et al.* (2016) assume uptake coefficients of 0.2 and 0.1 for HNO_3 and NH_3 respectively. On another note, if γ is used to tune the $NH_4{\cdot}NO_3$ concentrations to observations in future then existing biases in precursor gases (HNO_3 and NH_3), in terms of emissions and atmospheric processes, should first be evaluated and addressed. For instance, the curious surplus of simulated NH_3 at night at UK sites (Figure S9 in the Supplement) may be rectified by imposing a diurnal cycle on NH_3 emissions based on number of daylight hours, as implemented by Park *et al.* (2004). Bian *et al.* (2017) also highlight the importance of accurately simulating NH_3 dissolution in cloud droplets, which may be oversimplified in the UM owing to the ubiquitous assumption of a cloud droplet pH of 5 in UKCA.

This study has also highlighted a potential overestimate of NH_3 emissions in Europe in the CMIP6 emissions inventory, as also posited by Druge *et al.* (2019). An accurate NH_3 and NO_x emissions inventory is vital for a proficient simulation of NH_4 and NO_3 concentrations. HNO_3 concentrations also appear to be overestimated over the western US (Fig. 5) in these

simulations, which may emanate from an oversimplification of heterogeneous N_2O_5 chemistry in UKCA Strattrop1.0, given that the uptake coefficient in that reaction is uniformly set to 0.1 (Archibald *et al.*, 2020). Other simplifications such as uniformly assuming that mineral dust constitutes 5 % Ca^{2+} per mass and that the alkalinity of sea-salt may be titrated indefinitely may result in errors in coarse-mode NO_3 concentrations [Remy *et al.*, 2019]. Lastly, the assumption that HNO_3 and NH_3 are only involved in condensation and evaporation and not in nucleation may need to be revisited given developments in the theory of new particle formation (NPF) (Lee *et al.*, 2019; Wang *et al*., 2020). If NPF is found to dominate NH_4NO_3 production at higher tropospheric altitudes than condensation-related production, then the dynamics of convective transport of NH_4NO_3 precursors will become important.

The differences between the simulated and observed concentrations in this study (Figs 5-7) may be attributed to the use of perpetual year-2000 conditions in these simulations; the coarse model resolution utilised here (N96); biases in HNO_3 and NH_3 emissions, chemistry, and deposition; deficiencies in the thermodynamic equilibrium approach; and due to the choice of a monotonic uptake coefficient. In particular, this study has shown that the HNO_3 uptake coefficient is an important parameter in the production of ammonium nitrate and assuming a monotonic value in climate models may be an oversimplified an approach given the high sensitivity of HNO_3 uptake to ambient aerosol composition. Future simulations would benefit from stronger observational constraints on the HNO_3 and NH_3 uptake rates as a function of aerosol composition, relative humidity, and temperature, perhaps from targeted laboratory studies.

In a follow-on study, we aim to evaluate the nitrate scheme in high-resolution UM simulations for specific meteorological case-studies in a manner analogous to Gordon *et al*. (2018) but over a UK-based domain. Additionally, we will replace the constant HNO_3 uptake coefficient in the new nitrate scheme with a volume-weighted value based on aerosol composition and relative humidity, and re-run the simulations using transient CMIP6-like atmosphere-only UM integrations. The next issue to address will be coupling NO_3 and NH_4 aerosol within the UKESM framework. At present, fixed nitrogen (NO_y + NH_x) deposition to the land-surface model (JULES) in UKESM is applied using offline deposition fields from the input4MIPs database (see Sellar *et al*. (2020) for further details). Meanwhile, the ocean biogeochemistry module in UKESM (MEDUSA2; Yool *et al*. (2003)) has a closed nitrogen budget thus obviating interactions with atmospheric nitrogen. With the addition of ammonium and nitrate aerosol to a future version of UKESM, we will aim to fully couple atmospheric fixed-nitrogen deposition with the land and ocean surfaces to permit a comprehensive closed-budget nitrogen cycle.

In conclusion, the addition of ammonium and nitrate aerosol to UKCA-mode in the UM is step-change in aerosol-modelling capability in the UK and will increase confidence in future simulations of aerosol forcing and regional air pollution episodes. Additionally, nitrate concentrations have been shown to be highly sensitive to the nitric acid uptake rate, paving a way for climate models to reduce outstanding biases in ammonium nitrate concentrations.

Code Availability

Due to intellectual property rights restrictions, we cannot provide either the source code or documentation papers for the UM. The Met Office Unified Model is available for use under licence. A number of research organisations and national meteorological services use the UM in collaboration with the Met Office to undertake basic atmospheric process research, produce forecasts, develop the UM code, and build and evaluate Earth system models. For further information on how to apply for a licence, see http://www.metoffice.gov.uk/research/modelling-systems/unified-model (last access: 16 April 2021). The nitrate scheme is now available on the 'trunk' (the Met Office's data repository) and is available for all future UM versions since vn11.8 in UKCA mode setup 10.

Data Availability

The UM data used to produce the figures is available from the Centre of Environmental Data Analysis (CEDA) (http://dx.doi.org/10.5285/0613b74ecc574fa7b6ac8a22838c5f81; last accessed 12/05/2021) and if used should be cited accordingly: Jones, A.C.; Hill, A.; Remy, S.; Abraham, N.L.; Dalvi, M.; Hardacre, C.; Hewitt, A.J.; Johnson, B.; Mulcahy, J.P.; Turnock, S. (2021): Exploring the sensitivity of atmospheric nitrate concentrations to nitric acid uptake rate using the Met Office's Unified Model: nitrate and nitric acid simulation data. NERC EDS Centre for Environmental Data Analysis, *date of citation*. https://catalogue.ceda.ac.uk/uuid/0613b74ecc574fa7b6ac8a22838c5f81

Competing Interests

The authors declare that they have no conflict of interest.

Author contributions

ACJ developed the nitrate scheme with assistance from AH, SR, NLA, MD, and AJH. ACJ performed the simulations with assistance from NLA and MD. ACJ, AH, CH, BJ, JM, and SR analysed the simulations and compared the results to observations. ACJ wrote the manuscript with assistance from all co-authors.

Acknowledgements

The authors would like to thank the Met Office and the UM team for providing the UM climate model; NASA for making the MODIS satellite data freely available; and EMEP, the United States Environment Protection Agency (EPA), and GASSP for making their concentration measurement data freely available. The authors thank the many scientists who have contributed data utilised in this evaluation. The authors would also like to thank Didier Hauglustaine, John Hemmings, Nicolas Bellouin,

Alexander Archibald, Paul Griffiths, Steve Rumbold, Michael Cotterell, and Paul Agnew for their comments and assistance throughout this project. Figures were produced using Python 3.6.10 (https://www.python.org/) and Iris 2.4.0 (https://scitools.org.uk/).

ACJ and AH are supported by the Clean Air programme which is jointly delivered by the Natural Environment Research Council (NERC) and the Met Office, with the Economic and Social Research Council (ESRC), Engineering and Physical Sciences Research Council (EPSRC), Innovate UK, Medical Research Council (MRC), National Physical Laboratory (NPL), Science and Technology Facilities Research Council (STFC), Department for Environment, Food and Rural Affairs (Defra), Department for Health and Social Care (DHSC), Department for Transport (DfT), Scottish Government and Welsh Government. AJH is supported by the Joint DECC/Defra Met Office Hadley Centre Climate Programme (GA01101). BJ is funded by the Met Office Hadley Centre Climate Programme funded by BEIS and Defra (GA01101). NLA is supported by NERC and NCAS through the ACSIS project. ST would like to acknowledge that support for this work came from the UK-China Research and Innovation Partnership Fund through the Met Office Climate Science for Service Partnership (CSSP) China as part of the Newton Fund.

References

Aas, W., Tsyro, S., Bieber, E., Bergström, R., Ceburnis, D., Ellermann, T., Fagerli, H., Frölich, M., Gehrig, R., Makkonen, U., Nemitz, E., Otjes, R., Perez, N., Perrino, C., Prévôt, A. S. H., Putaud, J.-P., Simpson, D., Spindler, G., Vana, M., and Yttri, K. E.: Lessons learnt from the first EMEP intensive measurement periods, Atmos. Chem. Phys., 12, 8073–8094, doi:10.5194/acp12-8073-2012, 2012.

Ackermann, I. J., Hass, H., Memmesheimer, M., Ziegenbein, C., and Ebel, A.: The parameterization of the sulfate-nitrate ammonia aerosol system in the long-range transport model EURAD, Meteorol. Atmos. Phys., 57, 101–114, 1995.

Ansari, A. S., and S. N. Pandis: Response of inorganic PM to precursor concentrations, Environ. Sci. Technol., 32, 2706–2714, 1998.

Archibald, A. T., O'Connor, F. M., Abraham, N. L., Archer-Nicholls, S., Chipperfield, M. P., Dalvi, M., Folberth, G. A., Dennison, F., Dhomse, S. S., Griffiths, P. T., Hardacre, C., Hewitt, A. J., Hill, R. S., Johnson, C. E., Keeble, J., Köhler, M. O., Morgenstern, O., Mulcahy, J. P., Ordóñez, C., Pope, R. J., Rumbold, S. T., Russo, M. R., Savage, N. H., Sellar, A., Stringer, M., Turnock, S. T., Wild, O., and Zeng, G.: Description and evaluation of the UKCA stratosphere–troposphere chemistry scheme (StratTrop vn 1.0) implemented in UKESM1, Geosci. Model Dev., 13, 1223–1266, https://doi.org/10.5194/gmd-13-1223-2020, 2020.

Atkinson, R.: Atmospheric Chemistry of VOCs and NOx, Atmos. Environ., 34, 2063–2101, https://doi.org/10.1016/S1352-2310(99)00460-4, 2000.

Ballard, S.S., Browder, J.S., and Ebersole, J.F.: Refractive index of special crystals and certain glasses, in American Institute of Physics Handbook, 3rd ed., McGraw-Hill, New York, 1972.

Bauer, S. E., Balkanski, Y., Schulz, M., Hauglustaine, D. A., and Dentener, F.: Global modeling of heterogeneous chemistry on mineral aerosol surfaces: influence on tropospheric ozone chemistry and comparison to observations, J. Geophys. Res., 109, D02304, doi:10.1029/2003JD003868, 2004.

Bauer, S. E., Koch, D., Unger, N., Metzger, S. M., Shindell, D. T., and Streets, D. G.: Nitrate aerosols today and in 2030: a global simulation including aerosols and tropospheric ozone, Atmos. Chem. Phys., 7, 5043–5059, doi:10.5194/acp-7-5043-2007, 2007.

Bauer, S. E., Tsigaridis, K., and Miller, R.: Significant atmospheric aerosol pollution caused by world food cultivation, Geophys. Res. Lett., 43, 5394–5400, doi:10.1002/2016GL068354., 2016.

Bellouin, N., Boucher, O., Haywood, J., Johnson, C., Jones, A., Rae, J., and Woodward, S.: Improved representation of aerosols for HadGEM2, Hadley Centre technical note 73, Hadley Centre, Met Office, Exeter, UK, available at: http://www.metoffice.gov.uk/media/pdf/8/f/HCTN_73.pdf, 42 pp., 2007.

Bellouin, N., Rae, J., Jones, A., Johnson, C., Haywood, J., and Boucher, O.: Aerosol forcing in the Climate Model Intercomparison Project (CMIP5) simulations by HadGEM2-ES and the role of ammonium nitrate, J. Geophys. Res.-Atmos., 116, D20206, https://doi.org/10.1029/2011jd016074, 2011.

Bellouin, N., Mann, G. W., Woodhouse, M. T., Johnson, C., Carslaw, K. S., and Dalvi, M.: Impact of the modal aerosol scheme GLOMAP-mode on aerosol forcing in the Hadley Centre Global Environmental Model, Atmos. Chem. Phys., 13, 3027–3044, https://doi.org/10.5194/acp-13-3027-2013, 2013.

Bellouin, N., Quaas, J., Gryspeerdt, E., Kinne, S., Stier, P., WatsonParris, D., Boucher, O., Carslaw, K., Christensen, M., Daniau, A.-L., Dufresne, J.-L., Feingold, G., Fiedler, S., Forster, P., Gettelman, A., Haywood, J., Lohmann, U., Malavelle, F., Mauritsen, T., McCoy, D., Myhre, G., Mülmenstädt, J., Neubauer, D., Possner, A., Rugenstein, M., Sato, Y., Schulz, M., Schwartz, S., Sourdeval, O., Storelvmo, T., Toll, V., Winker, D., and Stevens, B.: Bounding global aerosol radiative forcing of climate change, Rev. Geophys., 58, e2019RG000660, https://doi.org/10.1029/2019RG000660, 2020.

Benduhn, F., Mann, G. W., Pringle, K. J., Topping, D. O., McFiggans, G., and Carslaw, K. S.: Size-resolved simulations of the aerosol inorganic composition with the new hybrid dissolution solver HyDiS-1.0 – Description, evaluation and first global modelling results, Geosci. Model Dev., 9, 3875–3906, doi:10.5194/gmd-9-3875-2016, 2016.

Bian, H., Chin, M., Hauglustaine, D. A., Schulz, M., Myhre, G., Bauer, S. E., Lund, M. T., Karydis, V. A., Kucsera, T. L., Pan, X., Pozzer, A., Skeie, R. B., Steenrod, S. D., Sudo, K., Tsigaridis, K., Tsimpidi, A. P., and Tsyro, S. G.: Investigation of global particulate nitrate from the AeroCom phase III experiment, Atmos. Chem. Phys., 17, 12911–12940, https://doi.org/10.5194/acp-17-12911-2017, 2017.

Bouwman, A. F., Lee, D. S., Asman, W. A. H., Dentener, F. J., Van Der Hoek, K. W., and Olivier, J. G. J.: A Global High-Resolution Emission Inventory for Ammonia, Global Biogeochem. Cy., 11, 561–587, https://doi.org/10.1029/97GB02266, 1997.

Buchard, V., Randles, C. A., da Silva, A. M., Darmenov, A., Colarco, P. R., Govindaraju, R., Ferrare, R., Hair, J., Beyersdorf, A. J., Ziemba, L. D., Yu, H., Buchard, V., Randles, C. A., Silva, A. M. da, Darmenov, A., Colarco, P. R., Govindaraju, R., Ferrare, R., Hair, J., Beyersdorf, A. J., Ziemba, L. D., and Yu, H.: The MERRA-2 Aerosol Reanalysis, 1980 Onward. Part II: Evaluation and Case Studies, J. Clim., 30, 6851–6872, https://doi.org/10.1175/JCLI-D-16-0613.1, 2017.

Carn, S. A., Fioletov, V. E., McLinden, C. A., Li, C., and Krotkov, N. A.: A decade of global volcanic SO2 emissions measured from space, Sci. Rep., 7, 44095, https://doi.org/10.1038/srep44095, 2017.

Cleaver, B., Rhodes, E., and Ubbelohde, A. R.: Studies of phase transformations in nitrates and nitrites I. Changes in ultra-violet absorption spectra on melting, Proc. R. Soc. London, 276, 437-453, https://doi.org/10.1098/rspa.1963.0217, 1963.

Cotterell, M. I., Willoughby, R. E., Bzdek, B. R., Orr-Ewing, A. J., and Reid, J. P.: A complete parameterisation of the relative humidity and wavelength dependence of the refractive index of hygroscopic inorganic aerosol particles, Atmos. Chem. Phys., 17, 9837–9851, https://doi.org/10.5194/acp-17-9837-2017, 2017.

Crutzen, P. J.: The influence of nitrogen oxides on the atmospheric ozone content, Q. J. Roy. Meteorol. Soc., 96, 320–325, doi:10.1002/qj.49709640815, 1970.

Department for Environment, Food and Rural Affairs (DEFRA): Report: Fine Particulate Matter (PM2.5) in the United Kingdom, Available here: https://uk-air.defra.gov.uk/library/reports?report_id=727, pp. 203, Published: 14/12/2012, DEFRA, London, UK, 2012.

Drugé, T., Nabat, P., Mallet, M., and Somot, S.: Model simulation of ammonium and nitrate aerosols distribution in the Euro-Mediterranean region and their radiative and climatic effects over 1979–2016, Atmos. Chem. Phys., 19, 3707–3731, https://doi.org/10.5194/acp-19-3707-2019, 2019.

Fairlie, T. D., Jacob, D. J., Dibb, J. E., Alexander, B., Avery, M. A., van Donkelaar, A., and Zhang, L.: Impact of mineral dust on nitrate, sulfate, and ozone in transpacific Asian pollution plumes, Atmos. Chem. Phys., 10, 3999–4012, doi:10.5194/acp-10-3999-2010, 2010.

Feng, Y. and Penner, J. E.: Global modeling of nitrate and ammonium: Interaction of aerosols and tropospheric chemistry, J. Geophys. Res.-Atmos., 112, D01304, https://doi.org/10.1029/2005jd006404, 2007.

Feng, L., Smith, S. J., Braun, C., Crippa, M., Gidden, M. J., Hoesly, R., Klimont, Z., van Marle, M., van den Berg, M., and van der Werf, G. R.: The generation of gridded emissions data for CMIP6, Geosci. Model Dev., 13, 461–482, https://doi.org/10.5194/gmd-13-461-2020, 2020

Finkelstein, P., Ellestad, T., Clarke, J., Meyers, T., Schwede, D., Hebert, E., and Neal, J.: Ozone and sulfur dioxide dry deposition to forests: Observations and model evaluation, J. Geophys. Res.-Atmos, 105, 15, 365–377, https://doi.org/10.1029/2000JD900185, 2000.

Fortems-Cheiney, A., Dufour, G., Hamaoui-Laguel, L., Foret, G., Siour, G., Van Damme, M., Meleux, F., Coheur, P.-F., Clerbaux, C., Clarisse, L., Favez, O., Wallasch, M., and Beekmann, M.: Unaccounted variability in NH3 agricultural sources detected by IASI contributing to European spring haze episode, Geophys. Res. Lett., 43, 5475–5482, https://doi.org/10.1002/2016GL069361, 2016.

Fuchs, N. A. and Sutugin, A. G.: Highly Dispersed Aerosols, Butterworth-Heinemann, Newton, Mass., USA, 105, 1970.

Gerber, H. E.: Relative-humidity parameterization of the Navy Aerosol Model (NAM), NRL Report 8956, Naval Research Laboratory, Washington, DC, 1985.

Giannakis, E., Kushta, J., Bruggeman, A., and Lelieveld, J.: Costs and benefits of agricultural ammonia emission abatement options for compliance with European air quality regulations, Environ. Sci. Eur., 31:93, https://doi.org/10.1186/s12302-019-0275-0, 2019.

Giannakopoulos, C., Chipperfield, T., Law, K., and Pyle, J.: Validation and intercomparison of wet and dry deposition schemes using Pb-210 in a global three-dimensional off-line chemical transport model, J. Geophys. Res., 104, 23761–23784, 1999.

Giorgi, F.: Climate change hot-spots, Geophys. Res. Lett., 33, L08707, https://doi.org/10.1029/2006GL025734, 2006.

Gordon, H., Field, P. R., Abel, S. J., Dalvi, M., Grosvenor, D. P., Hill, A. A., Johnson, B. T., Miltenberger, A. K., Yoshioka, M., and Carslaw, K. S.: Large simulated radiative effects of smoke in the south-east Atlantic, Atmos. Chem. Phys., 18, 15261–15289, https://doi.org/10.5194/acp-18-15261-2018, 2018.

Gosse, S. F., Wang, M., Labrie, D., and Chylek, P.: Imaginary part of the refractive index of sulfates and nitrates in the 0.7–2.6 μm spectral region, Appl. Opt., 36, 16, 3622–3634, 1997.

Granier, C., Bessagnet, B., Bond, T., D'Angiola, A., Denier van der Gon, H., Frost, G. J., Heil, A., Kaiser, J. W., Kinne, S., Klimont, Z., Kloster, S., Lamarque, J.-F., Liousse, C., Masui, T., Meleux, F., Mieville, A., Ohara, T., Raut, J.-C., Riahi, K., Schultz, M. G., Smith, S. J., Thompson, A., van Aardenne, J., van der Werf, G. R., and van Vuuren, D. P.: Evolution of anthropogenic and biomass burning emissions of air pollutants at global and regional scales during the 1980–2010 period, Clim. Change, 109, 163–190, https://doi.org/10.1007/s10584-011-0154-1, 2011.

Hardacre, C., Mulcahy, J. P., Pope, R., Jones, C. G., Rumbold, S. R., Li, C., and Turnock, S. T.: Evaluation of SO2, SO4(2-) and an updated SO2 dry deposition parameterization in UKESM1, Atmos. Chem. Phys. Discuss., https://doi.org/10.5194/acp-2021-238, 2021.

Hauglustaine, D. A., Balkanski, Y., and Schulz, M.: A global model simulation of present and future nitrate aerosols and their direct radiative forcing of climate, Atmos. Chem. Phys., 14, 11031– 11063, https://doi.org/10.5194/acp-14-11031-2014, 2014.

Hemmings, J., and Savage, N.: An Initial Evaluation of the GLOMAP-mode Aerosol Scheme for UK Air-Quality Forecasting with AQUM, Met Office Weather Science Technical Report No. 632, August 2018, pp. 70, Available here: https://www.metoffice.gov.uk/research/library-and-archive/publications/science/weather-science-technical-reports, Met Office, Exeter, UK, 2018.

Hoesly, R. M., Smith, S. J., Feng, L., Klimont, Z., Janssens-Maenhout, G., Pitkanen, T., Seibert, J. J., Vu, L., Andres, R. J., Bolt, R. M., Bond, T. C., Dawidowski, L., Kholod, N., Kurokawa, J.-I., Li, M., Liu, L., Lu, Z., Moura, M. C. P., O'Rourke, P. R., and Zhang, Q.: Historical (1750–2014) anthropogenic emissions of reactive gases and aerosols from the Community Emissions Data System (CEDS), Geosci. Model Dev., 11, 369–408, https://doi.org/10.5194/gmd-11-369-2018, 2018.

Hsu, N. C., Jeong, M.-J., Bettenhausen, C., Sayer, A. M., Hansell, R., Seftor, C. S., Huang, J., and Tsay S.-C.: Enhanced Deep Blue aerosol retrieval algorithm: The second generation, J. Geophys. Res.-Atmos., 118, 9296–9315, https://doi.org/10.1002/jgrd.50712, 2013.

Ivlev, L. S. and Popova, S. I.: Optical constants of substances of atmospheric aerosol, Sov. Phys. J., 15, 703–707, https://doi.org/10.1007/BF00893039, 1972.

Jacobson, M.: Numerical techniques to solve condensational and dissolutional growth equations when growth is coupled to reversible aqueous reactions, Aerosol Sci. Technol., 27, 491–498, doi:10.1080/02786829708965489,1997.

Jacobson, M. Z.: Isolating nitrated and aromatic aerosols and nitrated aromatic gases as sources of ultraviolet light absorption, J. Geophys. Res., 104, 3527–3542, https://doi.org/10.1029/1998JD100054, 1999.

Jarzembski, M. A., Norman, M. L., Fuller, K. A., Srivastava, V., and Cutten, D. R.: Complex refractive index of ammonium nitrate in the 2–20 μm spectral range, Appl. Optics, 42, 922–930, https://doi.org/10.1364/AO.42.000922, 2003.

Jimenez, J. L., Canagaratna, M. R., Donahue, N. M., Prevot, A. S. H., Zhang, Q., Kroll, J. H., DeCarlo, P. F., Allan, J. D., Coe, H., Ng, N. L., Aiken, A. C., Docherty, K. S., Ulbrich, I. M., Grieshop, A. P., Robinson, A. L., Duplissy, J., Smith, J. D., Wilson, K. R., Lanz, V. A., Hueglin, C., Sun, Y. L., Tian, J., Laaksonen, A., Raatikainen, T., Rautiainen, J., Vaattovaara, P., Ehn, M., Kulmala, M., Tomlinson, J. M., Collins, D. R., Cubison, M. J., Dunlea, E. J., Huffman, J. A., Onasch, T. B., Alfarra, M. R., Williams, P. I., Bower, K., Kondo, Y., Schneider, J., Drewnick, F., Borrmann, S., Weimer, S., Demerjian, K., Salcedo, D., Cottrell, L., Griffin, R., Takami, A., Miyoshi, T., Hatakeyama, S., Shimono, A., Sun, J. Y., Zhang, Y. M., Dzepina, K., Kimmel, J. R., Sueper, D., Jayne, J. T., Herndon, S. C., Trimborn, A. M., Williams, L. R., Wood, E. C., Middlebrook, A. M., Kolb, C. E., Baltensperger, U., and Worsnop, D. R.: Evolution of organic aerosols in the atmosphere, Science, 326, 5959, 1525– 1529, doi:10.1126/science.1180353, 2009.

Kucera, V., and Fitz, S.: Direct and indirect air pollution effects on materials including cultural monuments, Water Air Soil Pollut., 85, pp. 153-165, https://doi.org/10.1007/BF00483697, 1995.

Lee, S.-H., Gordon, H., Yu, H. ,Lehtipalo, K., Haley, R., Li, Y., and Zhang, R.: New particle formation in the atmosphere: From molecular clusters to global climate. J. Geophys. Res.-Atmos., 124, 7098–7146. https://doi.org/10.1029/2018JD029356, 2019.

Lelieveld, J., Evans, J. S., Fnais, M., Giannadaki, D., and Pozzer, A.: The contribution of outdoor air pollution sources to premature mortality on a global scale, Nature, 525, 367–371, doi:10.1038/nature15371, 2015.

Levy, R. C., Mattoo, S., Munchak, L. A., Remer, L. A., Sayer, A. M., Patadia, F., and Hsu, N. C.: The Collection 6 MODIS aerosol products over land and ocean, Atmos. Meas. Tech., 6, 2989–3034, https://doi.org/10.5194/amt-6-2989-2013, 2013.

Li, W. J. and Shao, L. Y.: Observation of nitrate coatings on atmospheric mineral dust particles, Atmos. Chem. Phys., 9, 1863–1871, doi:10.5194/acp-9-1863-2009, 2009.

Li, Y., Schichtel, B. A., Walker, J. T., Schwede, D. B., Chen, X., Lehmann, C. M. B., Puchalski, M. A., Gay, D. A., and Collett, J. L.: Increasing importance of deposition of reduced nitrogen in the United States, P. Natl. Acad. Sci. USA, 113, 5874–5879, doi:10.1073/pnas.1525736113, 2016.

Liao, H., Adams, P. J., Chung, S. H., Seinfeld, J. H., Mickley, L. J., and Jacob, D. J.: Interactions between tropospheric chemistry and aerosols in a unified general circulation model, J. Geophys. Res., 108, 4001, doi:10.1029/2001JD001260, 2003.

Lovett, G. M., Tear, T. H., Evers, D. C., Findlay, S. E. G., Cosby, B. J., Dunscomb, J. K., Driscoll, C. T., and Weathers, K. C.: Effects of air pollution on ecosystems and biological diversity in the eastern United States, Ann. N. Y. Acad. Sci., 1162, 99-135, doi:10.1111/j.1749-6632.2009.04153.x, 2009.

Makar, P. A., Wiebe, H. A., Staebler, R. M., Li, S.-M., and Anlauf, K.: Measurement and modelling of particle nitrate formation, J. Geophys. Res.-Atmos., 103, D11, 13 095–13 110, https://doi.org/10.1029/98JD00978, 1998.

Mann, G. W., Carslaw, K. S., Spracklen, D. V., Ridley, D. A., Mankte low, P. T., Chipperfield, M. P., Pickering, S. J., and Johnson, C. E.: Description and evaluation of GLOMAP-mode: a modal global aerosol microphysics mo del for the UKCA composition-climate model, Geosci. Model Dev., 3, 519–551, https://doi.org/10.5194/gmd-3-519-2010, 2010.

McDuffie, E. E., Smith, S. J., O'Rourke, P., Tibrewal, K., Venkataraman, C., Marais, E. A., Zheng, B., Crippa, M., Brauer, M., and Martin, R. V.: A global anthropogenic emission inventory of atmospheric pollutants from sector- and fuel-specific

sources (1970–2017): an application of the Community Emissions Data System (CEDS), Earth Syst. Sci. Data, 12, 3413–3442, https://doi.org/10.5194/essd-12-3413-2020, 2020.

Metzger, S., Dentener, F., Pandis, S., and Lelieveld, J.: Gas/aerosol partitioning: 1. A computationally efficient model, J. Geophys. Res., 107, D164312, https://doi.org/10.1029/2001JD001102, 2002.

Monks, P. S., Granier, C., Fuzzi, S., Stohl, A., Williams, M. L., Akimoto, H., Amann, M., Baklanov, A., Baltensperger, U., Bey, I., Blake, N., Blake, R. S., Carslaw, K., Cooper, O. R., Dentener, F., Fowler, D., Fragkou, E., Frost, G. J., Generoso, S., Ginoux, P., Grewe, V., Guenther, A., Hansson, H. C., Henne, S., Hjorth, J., Hofzumahaus, A., Huntrieser, H., Isaksen, I. S. A., Jenkin, M. E., Kaiser, J., Kanakidou, M., Klimont, Z., Kulmala, M., Laj, P., Lawrence, M. G., Lee, J. D., Liousse, C., Maione, M., McFiggans, G., Metzger, A., Mieville, A., Moussiopoulos, N., Orlando, J. J., O'Dowd, C. D., Palmer, P. I., Parrish, D. D., Petzold, A., Platt, U., Poeschl, U., Prevot, A. S. H., Reeves, C. E., Reimann, S., Rudich, Y., Sellegri, K., Steinbrecher, R., Simpson, D., ten Brink, H., Theloke, J., van der Werf, G. R., Vautard, R., Vestreng, V., Vlachokostas, C., and von Glasow, R.: Atmospheric composition change – global and regional air quality, Atmos. Environ., 43, 5268–5350, doi:10.1016/j.atmosenv.2009.08.021, 2009.

Mozurkewich, M.: The dissociation constant of ammonium nitrate and its dependence on temperature, relative humidity and particle size, Atmos. Environ. A-Gen., 27, 261–270, 1993.

Mulcahy, J. P., Johnson, C., Jones, C. G., Povey, A. C., Scott, C. E., Sellar, A., Turnock, S. T., Woodhouse, M. T., Abraham, N. L., Andrews, M. B., Bellouin, N., Browse, J., Carslaw, K. S., Dalvi, M., Folberth, G. A., Glover, M., Grosvenor, D. P., Hardacre, C., Hill, R., Johnson, B., Jones, A., Kipling, Z., Mann, G., Mollard, J., O'Connor, F. M., Palmiéri, J., Reddington, C., Rumbold, S. T., Richardson, M., Schutgens, N. A. J., Stier, P., Stringer, M., Tang, Y., Walton, J., Woodward, S., and Yool, A.: Description and evaluation of aerosol in UKESM1 and HadGEM3-GC3.1 CMIP6 historical simulations, Geosci. Model Dev., 13, 6383–6423, https://doi.org/10.5194/gmd-13-6383-2020, 2020.

Myhre, G., Grini, A., and Metzger, S.: Modelling of nitrate and ammonium-containing aerosols in presence of sea salt, Atmos. Chem. Phys., 6, 4809–4821, http://www.atmos-chem-phys.net/6/4809/2006/, 2006.

Myhre, G., Samset, B. H., Schulz, M., Balkanski, Y., Bauer, S., Berntsen, T. K., Bian, H., Bellouin, N., Chin, M., Diehl, T., Easter, R. C., Feichter, J., Ghan, S. J., Hauglustaine, D., Iversen, T., Kinne, S., Kirkevåg, A., Lamarque, J.-F., Lin, G., Liu, X., Lund, M. T., Luo, G., Ma, X., van Noije, T., Penner, J. E., Rasch, P. J., Ruiz, A., Seland, Ø., Skeie, R. B., Stier, P., Takemura, T., Tsigaridis, K., Wang, P., Wang, Z., Xu, L., Yu, H., Yu, F., Yoon, J.-H., Zhang, K., Zhang, H., and Zhou, C.: Radiative

forcing of the direct aerosol effect from AeroCom Phase II simulations, Atmos. Chem. Phys., 13, 1853–1877, https://doi.org/10.5194/acp13-1853-2013, 2013.

Nenes, A., Pandis, S. N., and Pilinis, C.: ISORROPIA: A new thermodynamic equilibrium model for multiphase multicomponent inorganic aerosols, Aquat. Geochem., 4, 123–152, https://doi.org/10.1023/A:1009604003981, 1998.

Palik, E. D.; Khanna, R. Sodium Nitrate (NaNO3). In Handbook of Optical Constants; Palik, E. D., Ed.; Academic Press: New York, 1998; Vol. 3, p 871, 1998.

Park, R. J., Jacob, D. J., Field, B. D., Yantosca, R. M., and Chin, M.: Natural and transboundary pollution influences on sulfate-nitrate-ammonium aerosols in the United States: Implications for policy, J. Geophys. Res., 109, D15204, doi:10.1029/2003JD004473, 2004.

Paulot, F., Ginoux, P., Cooke, W. F., Donner, L. J., Fan, S., Lin, M.-Y., Mao, J., Naik, V., and Horowitz, L. W.: Sensitivity of nitrate aerosols to ammonia emissions and to nitrate chemistry: implications for present and future nitrate optical depth, Atmos. Chem. Phys., 16, 1459–1477, https://doi.org/10.5194/acp16-1459-2016, 2016.

Putaud, J. P., Raes, F., Van Dingenen, R., Bruggemann, E., Faccini, M. C., Decesari, S., Fuzzi, S., Gehrig, R., Huglin, C., Laj, P., Lorbeer, G., Maenhaut, W., Mihalopoulos, N., Muller, K., Querol, X., Rodriguez, S., Schneider, J., Spindler, G., ten Brink, H., Tørseth, K., and Wiedensohler, A.: A European aerosol phenomenology 2: chemical characteristics of particulate matter at kerbside, urban, rural and background sites in Europe, Atmos. Environ., 38, 2579–2595, 2004

Randles, C. A., da Silva, A. M., Buchard, V., Colarco, P. R., Darmenov, A., Govindaraju, R., Smirnov, A., Holben, B., Ferrare, R., Hair, J., Shinozuka, Y., Flynn, C. J., Randles, C. A., Silva, A. M. da, Buchard, V., Colarco, P. R., Darmenov, A., Govindaraju, R., Smirnov, A., Holben, B., Ferrare, R., Hair, J., Shinozuka, Y., and Flynn, C. J.: The MERRA-2 Aerosol Reanalysis, 1980 Onward. Part I: System Description and Data Assimilation Evaluation, J. Clim., 30, 6823–6850, https://doi.org/10.1175/JCLI-D16-0609.1, 2017.

Reddington, C. L., Carslaw, K. S., Stier, P., Schutgens, N., Coe, H., Liu, D., Allan, J., Browse, J., Pringle, K. J., Lee, L. A., Yoshioka, M., Johnson, J. S., Regayre, L. A., Spracklen, D. V., Mann, G. W., Clarke, A., Hermann, M., Henning, S., Wex, H., Kristensen, T. B., Leaitch, W. R., Pöschl, U., Rose, D., Andreae, M. O., Schmale, J., Kondo, Y., Oshima, N., Schwarz, J. P., Nenes, A., Anderson, B., Roberts, G. C., Snider, J. R., Leck, C., Quinn, P. K., Chi, X., Ding, A., Jimenez, J. L., and Zhang, Q.: The global aerosol synthesis and science project (GASSP): Measurements and modeling to reduce uncertainty, B. Am. Meteorol. Soc., 98, 1857–1877, https://doi.org/10.1175/BAMS-D-15-00317.1, 2017.

Rémy, S., Kipling, Z., Flemming, J., Boucher, O., Nabat, P., Michou, M., Bozzo, A., Ades, M., Huijnen, V., Benedetti, A., Engelen, R., Peuch, V.-H., and Morcrette, J.-J.: Description and evaluation of the tropospheric aerosol scheme in the European Centre for Medium-Range Weather Forecasts (ECMWF) Integrated Forecasting System (IFS-AER, cycle 45R1), Geosci. Model Dev., 12, 4627–4659, https://doi.org/10.5194/gmd-12-4627-2019, 2019.

Sander, S. P., Abbatt, J., Barker, J. R., Burkholder, J. B., Friedl, R. R., Golden, D. M., Huie, R. E., Kolb, C. E., Kurylo, M. J., Moortgat, G. K., Orkin, V. L., and Wine, P. H.: Chemical Kinetics and Photochemical Data for Use in Atmospheric Studies, Evaluation No. 17, JPL Publication 10-6, Jet Propulsion Laboratory, Pasadena, 2011.

Savage, N. H., Agnew, P., Davis, L. S., Ordóñez, C., Thorpe, R., Johnson, C. E., O'Connor, F. M., and Dalvi, M.: Air quality modelling using the Met Office Unified Model (AQUM OS24-26): model description and initial evaluation, Geosci. Model Dev., 6, 353–372, doi:10.5194/gmd-6-353-2013, 2013.

Schwartz, S. E.: Mass transport considerations pertinent to aqueous phase reactions of gases in liquid-water clouds, in: Chemistry of Multiphase Atmospheric Systems, edited by: Jaeschke, W., 415–471, Springer, New York, 1986.

Seinfeld, J. H. and Pandis, S. N.: Atmospheric Chemistry and Physics: From Air Pollution to Climate Change, John, Wiley & Sons, Inc., 1998.

Sellar, A., Jones, C. G., Mulcahy, J. P., Tang, Y., Yool, A., Wiltshire, A., O'Connor, F. M., Stringer, M., Hill, R., Palmieri, J., Woodward, S., de Mora, L., Kuhlbrodt, T., Rumbold, S., Kelley, D. I., Ellis, R., Johnson, C. E., Walton, J., Abraham, N. L., Andrews, M. B., Andrews, T., Archibald, A. T., Berthou, S., Burke, E., Blockley, E., Carslaw, K., Dalvi, M., Edwards, J., Folberth, G. A., Gedney, N., Griffiths, P. T., Harper, A. B., Hendry, M. A., Hewitt, A. J., Johnson, B., Jones, A., Jones, C. D., Keeble, J., Liddicoat, S., Morgenstern, O., Parker, R. J., Predoi, V., Robertson, E., Siahaan, A., Smith, R. S., Swaminathan, R., Woodhouse, M., Zeng, G., and Zerroukat, M.: UKESM1: Description and evaluation of the UK Earth System Model, J. Adv. Model. Earth Syst., https://doi.org/10.1029/2019MS001739, 2019.

Sellar, A., Walton, J., Jones, C. G., Wood, R., Abraham, N. L., Andrejczuk, M., Andrews, M. B., Andrews, T., Archibald, A. T., Dyson, H., Elkington, M., Ellis, R., Florek, P., Good, P., Gohar, L., Haddad, S., Hardiman, S. C., Hogan, E., Iwi, A., Jones, C. D., Johnson, B., Kelley, D. I., Kettleborough, J., Knight, J. R., Köhler, M. 5 O., Kuhlbrodt, T., Liddicoat, S., Linova-Pavlova, I., Mizielinski, M. S., Morgenstern, O., Mulcahy, J., Neininger, E., O'Connor, F. M., Petrie, R., Ridley, J., Rioual, J.-C., Roberts, M., Robertson, E., Rumbold, S., Seddon, J., Shepherd, H., Shim, S., Stephens, A., Teixeira, J. C., Tang, Y.,

Williams, J., and Wiltshire, A.: Implementation of UK Earth system models for CMIP6, J. Adv. Model. Earth Syst., 12, e2019MS001946. https://doi.org/10.1029/2019MS001946, 2020.

Shah, V., Jaeglé, L., Thornton, J. A., Lopez-Hilfiker, F. D., Lee, B. H., Schroder, J. C., Campuzano-Jost, P., Jimenez, J. L., Guo, H., Sullivan, A. P., Weber, R. J., Green, J. R., Fiddler, M. N., Bililign, S., Campos, T. L., Stell, M., Weinheimer, A. J., Montzka, D. D., and Brown, S. S.: Chemical feedbacks weaken the wintertime response of particulate sulfate and nitrate to emissions reductions over the eastern United States, P. Natl. Acad. Sci. USA, 115, 8110, https://doi.org/10.1073/pnas.1803295115, 2018.

Smith, C., Hill, A. K., and Torrente-Murciano, L.: Current and future role of Haber–Bosch ammonia in a carbon-free energy landscape, Energy Environ. Sci., doi: 10.1039/c9ee02873k, 13, 331, 2020.

Torseth, K., Aas, W., Breivik, K., Fjaeraa, A. M., Fiebig, M., Hjellbrekke, A. G., Myhre, C. L., Solberg, S., and Yttri, K. E.: Introduction to the European Monitoring and Evaluation Programme (EMEP) and observed atmospheric composition change during 1972-2009, Atmos. Chem. Phys., 12, 5447–5481, https://doi.org/10.5194/acp-12-5447-2012, 2012.

Turnock, S. T., Allen, R. J., Andrews, M., Bauer, S. E., Deushi, M., Emmons, L., Good, P., Horowitz, L., John, J. G., Michou, M., Nabat, P., Naik, V., Neubauer, D., O'Connor, F. M., Olivié, D., Oshima, N., Schulz, M., Sellar, A., Shim, S., Takemura, T., Tilmes, S., Tsigaridis, K., Wu, T., and Zhang, J.: Historical and future changes in air pollutants from CMIP6 models, Atmos. Chem. Phys., 20, 14547–14579, https://doi.org/10.5194/acp-20-14547-2020, 2020.

Twigg, M. M., Ilyinskaya, E., Beccaceci, S., Green, D. C., Jones, M. R., Langford, B., Leeson, S. R., Lingard, J. J. N., Pereira, G. M., Carter, H., Poskitt, J., Richter, A., Ritchie, S., Simmons, I., Smith, R. I., Tang, Y. S., Van Dijk, N., Vincent, K., Nemitz, E., Vieno, M., and Braban, C. F.: Impacts of the 2014–2015 Holuhraun eruption on the UK atmosphere, Atmos. Chem. Phys., 16, 11415–11431, https://doi.org/10.5194/acp-16-11415-2016, 2016.

van Marle, M. J. E., Kloster, S., Magi, B. I., Marlon, J. R., Daniau, A.-L., Field, R. D., Arneth, A., Forrest, M., Hantson, S., Kehrwald, N. M., Knorr, W., Lasslop, G., Li, F., Mangeon, S., Yue, C., Kaiser, J. W., and van der Werf, G. R.: Historic global biomass burning emissions for CMIP6 (BB4CMIP) based on merging satellite observations with proxies and fire models (1750–2015), Geosci. Model Dev., 10, 3329–3357, https://doi.org/10.5194/gmd-10-3329-2017, 2017.

Vlasenko, A., Sjogren, S., Weingartner, E., Stemmler, K., Gaggeler, H. W., and Ammann, M.: Effect of humidity on nitric acid uptake to mineral dust aerosol particles, Atmos. Chem. Phys., 6, 2147– 2160, doi:10.5194/acp-6-2147-2006, 2006.

Vinken, G. C. M., Boersma, K. F., Maasakkers, J. D., Adon, M., and Martin, R. V.: Worldwide biogenic soil NOx emissions inferred from OMI NO2 observations, Atmos. Chem. Phys., 14, 10363– 10381, doi:10.5194/acp-14-10363-2014, 2014.

Walters, D., Baran, A. J., Boutle, I., Brooks, M., Earnshaw, P., Edwards, J., Furtado, K., Hill, P., Lock, A., Manners, J., Morcrette, C., Mulcahy, J., Sanchez, C., Smith, C., Stratton, R., Tennant, W., Tomassini, L., Van Weverberg, K., Vosper, S., Willett, M., Browse, J., Bushell, A., Carslaw, K., Dalvi, M., Essery, R., Gedney, N., Hardiman, S., Johnson, B., Johnson, C., Jones, A., Jones, C., Mann, G., Milton, S., Rumbold, H., Sellar, A., Ujiie, M., Whitall, M., Williams, K., and Zerroukat, M.: The Met Office Unified Model Global Atmosphere 7.0/7.1 and JULES Global Land 7.0 configurations, Geosci. Model Dev., 12, 1909–1963, https://doi.org/10.5194/gmd-12-1909-2019, 2019.

Wang, M., Kong, W., Marten, R. *et al.*: Rapid growth of new atmospheric particles by nitric acid and ammonia condensation. Nature, 581**,** 184–189, https://doi.org/10.1038/s41586-020-2270-4, 2020

Weast, R.C.: CRC Handbook of Chemistry and Physics, 1971-1972: A Ready Reference Book of Chemical and Physical Data, 52nd ed., 1971.

Wexler, A. S. and Seinfeld, J. H.: The distribution of ammonium salts among a size and composition dispersed aerosol, Atmos. Environ., 24A, 1231–1246, 1990.

Womack, C. C., McDuffie, E. E., Edwards, P. M., Bares, R., Gouw, J. A. A., Docherty, K. S., Dubé, W. P., Fibiger, D. L., Franchin, A., Gilman, J. B., Goldberger, L., Lee, B. H., Lin, J. C., Long, R., Middlebrook, A. M., Millet, D. B., Moravek, A., Murphy, J. G., Quinn, P. K., Riedel, T. P., Roberts, J. M., Thornton, J. A., Valin, L. C., Veres, P. R., Whitehill, A. R., Wild, R. J., Warneke, C., Yuan, B., Baasandorj, M., and Brown, S. S.: An Odd Oxygen Framework for Wintertime Ammonium Nitrate Aerosol Pollution in Urban Areas: NOx and VOC Control as Mitigation Strategies, Geophys. Res. Lett., 46, 4971–4979, https://doi.org/10.1029/2019GL082028, 2019.

Woodward, S.: Modelling the atmospheric life cycle and radiative impact of mineral dust in the Hadley Centre climate model, J. Geophys. Res., 106, 18 155–18 166, 2001.

World Health Organisation (WHO): World health statistics 2020: monitoring health for the SDGs, sustainable development goals. Geneva: World Health Organization; 2020. Licence: CC BY-NC-SA 3.0 IGO, 2020.

Xiao, H.-W., Xiao, H.-Y., Shen, C.-Y., Zhang, Z.-Y., and Long, A.-M.: Chemical Composition and Sources of Marine Aerosol over the Western North Pacific Ocean in Winter, Atmosphere, 9, 298; doi:10.3390/atmos9080298, 2018.

Xu, L. and Penner, J. E.: Global simulations of nitrate and ammonium aerosols and their radiative effects, Atmos. Chem. Phys., 12, 9479–9504, https://doi.org/10.5194/acp-12-9479-2012, 2012.

Xu, R., Tian, H., Pan, S., Prior, S. A., Feng, Y., Batchelor, W. D., Chen, J., and Yang, J.: Global ammonia emissions from synthetic nitrogen fertilizer applications in agricultural systems: Empirical and process-based estimates and uncertainty, Glob. Change Biol., 25, 314–326, https://doi.org/10.1111/gcb.14499, 2019.

Yienger, J. J., and Levy, H.: Empirical model of global soil-biogenic NO_x emissions, J. Geophys. Res., 100(D6), 11447, https://doi.org/10.1029/95JD00370, 1995.

Yool, A., Popova, E. E., and Anderson, T. R.: MEDUSA-2.0: an intermediate complexity biogeochemical model of the marine carbon cycle for climate change and ocean acidification studies, Geosci. Model Dev., 6, 1767–1811, doi:10.5194/gmd-6-1767-2013, 2013.

Zaveri, R. A., Easter, R. C., Fast, J. D., and Peters, L. K.: Model for Simulating Aerosol Interactions and Chemistry (MOSAIC), J. Geophys. Res., 113, D13204, doi:10.1029/2007JD008782., 2007.

Zhong, Q., Shen, H., Yun, X., Chen, Y., Ren, Y., Xu, H., Shen, G., Du, W., Meng, J., Li, W., Ma, J., and Tao, S.: Global Sulfur Dioxide Emissions and the Driving Forces, Environ. Sci. Technol., 54, 6508−6517, https://dx.doi.org/10.1021/acs.est.9b07696, 2020.

Zhu, L., Henze, D. K., Bash, J. O., Cady-Pereira, K. E., Shephard, M. W., Luo, M., and Capps, S. L.: Sources and Impacts of Atmospheric NH_3: Current Understanding and Frontiers for Modeling, Measurements, and Remote Sensing in North America, Curr. Pollution Rep., 1, 95–116, DOI:10.1007/s40726-015-0010-4, 2015